RESEARCH ACTIVITIES

VACUUM-ULTRAVIOLET ABSORPTION SPECTRA OF CCl_3F and CCl_2F_2

Toshio IBUKI, Atsunari HIRAYA* and Kosuke SHOBATAKE*
Institute for Chemical Research, Kyoto University, Uji, Kyoto 611
*Institute for Molecular Science, Myodaiji, Okazaki 444

Chlorofluoromethanes such as CCl_3F and CCl_2F_2 are typical aerosol propellants and refrigerants, and recently they have used as dry or plasma echants. The role of halogenated methanes in photochemistry in the upper atmosphere has been debated since the stratospheric ozone layer may or may not be depleted by Cl atoms released through solar photolysis of chlorofluoromethanes. Because of the importance of the ozone layer as solar UV-radiation shield, many investigations of their absorption or photoreactions have been carried out, mostly at $\lambda > 170$ nm.

Figures 1 and 2 show the absorption and fluorescence excitation spectra of CCl_3F and CCl_2F_2, respectively, using an apparatus at the BL-2A station of UVSOR. The valence shell configuration of CCl_3F is $(3e)^4(5a_1)^2(4e)^4(5e)^4(1a_2)^2$.[1] Chlorine lone pair orbitals are of a_2, e, e and a_1 symmetries, the ionization potentials of which are in order 11.76, 12.13, 12.96 and

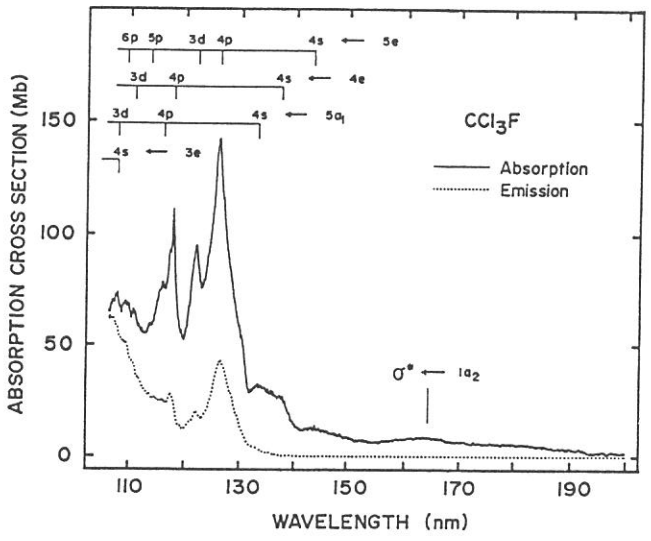

Fig. 1. Absorption and fluorescence excitation spectra of CCl_3F.

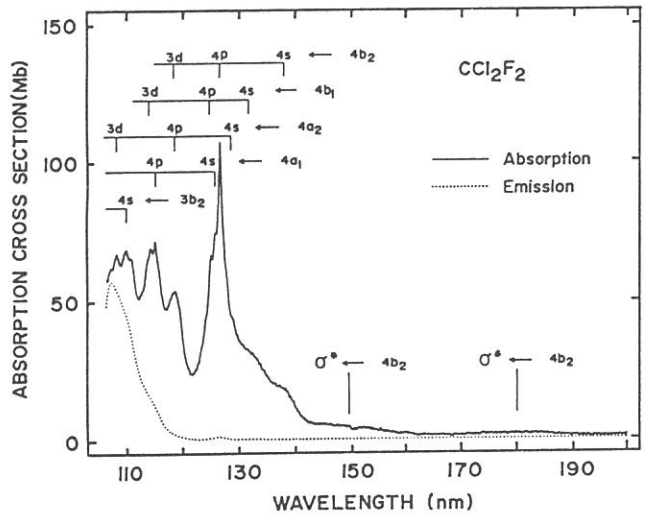

Fig. 2. Absorption and fluorescence excitation spectra of CCl_2F_2.

13.42 eV, respectively.[1] The next inner 3e orbital represents mainly the σ_{C-Cl} bonding electron with IP = 15.01 eV. Using these IP values, the Rydberg assignments are given in Fig. 1.

The electronic configuration of the outer shells of CCl_2F_2 is expressed as $(3b_2)^2(4a_1)^2(4a_2)^2(4b_1)^2(4b_2)^2$.[2] Adopting the published IPs of these orbitals,[2] the assignments of the Rydberg transitions are also given in Fig. 2.

The emitters are assigned as $CClF(\tilde{A}^1A'')$ and $CF_2(\tilde{A}^1B_1)$ radicals in the photodecomposition of CCl_3F and CCl_2F_2, respectively. The thresholds for the fluorescence strongly support the following processes:

$$CCl_3F + h\nu \rightarrow CClF(\tilde{A}) + 2Cl,$$
$$CCl_2F_2 + h\nu \rightarrow CF_2(\tilde{A}) + 2Cl.$$

The radiative lifetimes of the excited $\tilde{A}$ state of CClF and CF_2 are determined to be 650 ± 20 and 58 ± 2 ns, respectively.

References

1) M. R. Jardrny, L. Karlsson, L. Mattsson, and K. Siegbahn, Phys. Scri. 16, 235 (1977).

2) T. Cvitas, H. Güsten, and L. Klansinc, J. Chem. Phys. 67, 2687 (1977).

ABSORPTION AND FLUORESCENCE SPECTRA OF S_2Cl_2 AND $OSCl_2$

Ikuo TOKUE, Atsunari HIRAYA*, and Kosuke SHOBATAKE*

Department of Chemistry, Niigata University, Niigata 950-21
*Institute for Molecular Science, Myodaiji, Okazaki 444

Several photochemical studies have been made on S_2Cl_2[1] and $OSCl_2$[2,3] Time resolved spectroscopic studies of S_2Cl_2[1] in the near ultraviolet flash photolysis indicate that primary process is in the fission of the S-S bond following an $n-\pi^*$ or $n-\sigma^*$ transition:

$$S_2Cl_2 + h\nu \longrightarrow 2SCl. \qquad (1)$$

The excited states of SO, $A^3\Pi$ and $B^3\Sigma$, were found to be formed in the photodissociation of $OSCl_2$[3] at the Kr resonance lines. The primary process for producing of SO(A) near its threshold energy is

$$OSCl_2 + h\nu \longrightarrow SO(A) + 2Cl(^2P_{3/2}). \qquad (2)$$

In the present work, the photoabsorption cross section (c.s.) and fluorescence excitation spectrum of S_2Cl_2 and $OSCl_2$ in the vacuum ultraviolet (VUV) were measured. Fluorescence spectra from the excited fragments produced were observed in the 200-500 nm region in the experiment. All chemicals obtained commercially were vacuum-distilled and stored in a pyrex container. All data were measured at vapor pressure lower than 20 mTorr.

The photoabsorption c.s. of S_2Cl_2 as a function of wavelength in the 105-200 nm region are reproduced in fig. 1 with the fluorescence excitation spectrum. In the absorption spectrum several peaks are attributed to the HCl impurity; the concentration of HCl impurity is estimated to be $\simeq 5$ %. The experimental uncertainty in the absorption c.s. was estimated to be within ± 15 % of the given value. The fluorescence excitation spectrum in the 110-150 nm region follows closely the main features in the absorption c.s. Dispersed emission measured at the excitation wavelength of 113.0, 115.8 and 125.8 nm is shown in fig. 2. The spectral resolution of emission is 6 nm. Three emission bands are probably observed; namely, the relatively sharp bands centered at 256 and 316 nm and the broad band centered at 350 nm. Comparing with the assignment of the absorption spectrum by Donovan et al.[1], we concluded that the broad band centered at 350 nm is attributed to the $S_2(B-X)$ band. The threshold wavelength of incident photons for producing fluorescence measured by monitoring both the total emission and the emission at 320 ± 6 nm is 155.5 ± 0.6 nm; fluorescence from HCl impurity longer than 125 nm is negligible. The primary process for producing of $S_2(B)$ near

its threshold energy is

$$S_2Cl_2 + h\nu \longrightarrow S_2(B) + 2Cl(^2P_{3/2}). \qquad (3)$$

The minimum energy required for Reaction (3) is 7.99 eV(155.2 nm).

The photoabsorption c.s.and the fluorescence intensity of $OSCl_2$ as a function of wavelength in the 105-220 nm region have been measured. The absorption c.s. observed in the 115-135 nm region is found to be ≃ 25 % smaller than that reported by Okabe[3]. This is probably caused by the Cl_2, HCl and SO_2 impurities. The fluorescence excitation spectrum of $OSCl_2$ shows two peaks at 107 and 113 nm. The emission spectra with the spectral resolution of 6 nm were observed at the excitation wavelengths of 107±1 and 113±1 nm. The sharp band centered at 256 nm and the broad band in the 240-400 nm region are attributed to the SO(A-X) and SO(B-X) band, respectively. The threshold wavelengths of the excitation photons for producing the fluorescence measured by monitoring the total emission and the emission at 256±6 nm are 132.±0.6 and 130.6±0.6 nm, respectively. These are in good agreement with the value reported by Okabe[3].

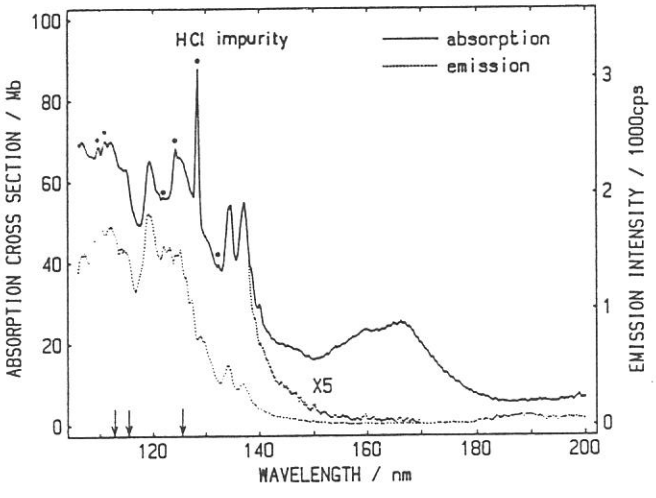

Fig. 1. The absorption c.s. and fluorescence excitation spectra of S_2Cl_2

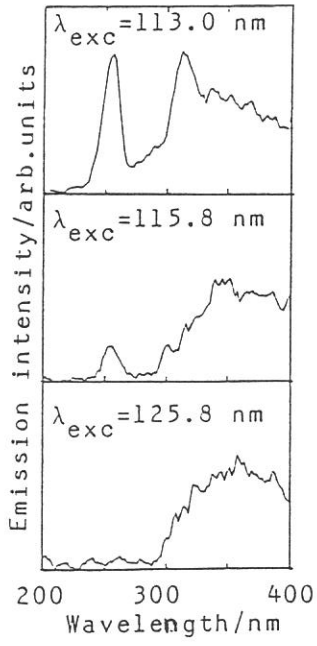

Fig. 2. Emission spectra produced from S_2Cl_2 at 113.0, 115.8 and 125.8 nm excitations

References

[1] R.J.Donovan, D.Husain and P.T.Jackson, Trans. Faraday Soc. 64, 1798 (1968); R.J.Donovan, D.Husain and C.D.Stevenson, ibid. 66, 1(1970).

[2] R.J.Donovan, D.Husain and P.T.Jackson, Trans. Faraday Soc. 65, 2930(1969).

[3] H. Okabe, J. Chem. Phys. 56, 3378(1972).

ISOTOPE EFFECT ON THE FLUORESCENCE CROSS SECTION FOR THE DISSOCIATIVE EXCITATION PROCESSES. II. CH_3OH AND ITS DEUTERATED COMPOUNDS.

Atsunari HIRAYA and Kosuke SHOBATAKE

Institute for Molecular Science, Myodaiji, Okazaki 444

In order to elucidate the conspicuous isotope effect on the quantum yield of $CN^*(A,B)$ formation in photodissociative excitation of CH_3CN and CD_3CN[1] by VUV light, fluorescence cross sections of CH_3OH and its deuterated compounds, in which CN group is replaced by OH or OD, have been investigated.

Figure 1 shows the absorption and fluorescence excitation spectra of CH_3OH and CD_3OD. The emission excitation spectrum was obtained by monitoring the total emission in the wavelength range 180 - 650 nm. Two emitting species are possible for the photodissociative excitation of CH_3OH, i.e. OH^* and CH_3O^*. The threshold wavelengths for the formation of OH^* and CH_3O^* are indicated by arrows in the fluorescence excitation spectra. The observed onsets of total emission for both compounds are in good agreement with the calculated threshold of 155 nm for $OH^*(OD^*)$ formation. Although the total emission excitation spectrum is a superposition of the excitation function of OH^* and CH_3O^*, the dispersed emission spectrum was found to be

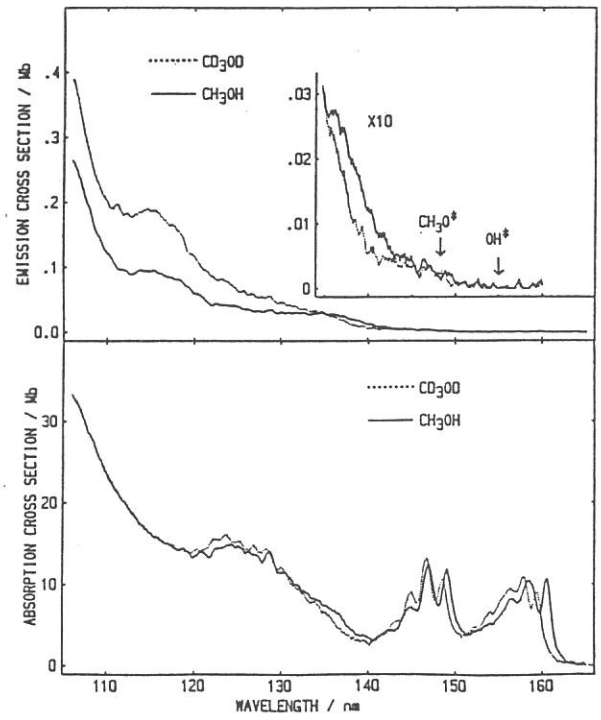

Figure 1. Absorption and total emission excitation spectra of CH_3OH (solid line) and CD_3OD (dotted line) in gas phase.

dominated by $OH^*(OD^*)$ emission band at 310nm. Therefore it can be said that the total emission excitation spectrum mainly represent the excitation function of OH^*.

The total emission cross section of CD_3OD is about a factor of two larger than that of CH_3OH in the shorter wavelength region than 134 nm. On the contrary, such a notable isotope effect was not found for CH_3OD within the experimental error. Therefore, it was concluded that the substitution of deuterium atoms for hydrogen atoms at methyl group enhances the formation of OH^*, as was already found for the formation of CN^* from CH_3CN and CD_3CN. The similar isotope effect observed for these two molecules, each having a different functional group OH or CN, strongly supports our previous model that such a conspicuous isotope effect on the emission cross section originates from the variation in the rates of other dissociation channels, which compete with OH^* or CN^* formation, and involve the motion of hydrogen (deuterium) atoms in the methyl group, i.e. C-H (C-D) rupture.

Because $CH_3O(^2A_1 - X^2E)$ emission extends from 280 to 450 nm, the excitation function of CH_3O^* can be obtained by monitoring emissions at wavelength longer than 350nm, as shown in Figure 2. These excitation functions of CH_3O^* are entirely different from both the absorption and the total emission excitation spectra. This implies that OH^* and CH_3O^* are formed via different electronic states. The observed isotope effect on the formation of CH_3O^* is quite different from that of OH^*. One can reasonably explain it in terms of the isotope effect on the competition between C-H bond and O-H bond ruptures.

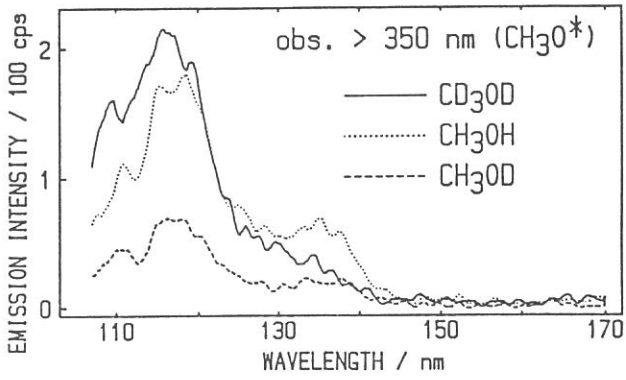

Figure 2. Emission excitation spectra obtained by monitoring longer wavelengths than 350nm

Reference

1) K. Shobatake et al., Ann. Rev. IMS 1984, p.96; UVSOR activity report 1984/85, p. 43.

ISOTOPE EFFECT ON THE FLUORESCENCE CROSS SECTION FOR THE DISSOCIATIVE EXCITATION PROCESSES. III. EVIDENCE OF CCl_2 FORMATION FROM $CHCl_3$ AND $CDCl_3$.

Atsunari HIRAYA, Toshio IBUKI*, and Kosuke SHOBATAKE

Institute for Molecular Science, Myodaiji, Okazaki 444
*Institute for Chemical Research, Kyoto Univ., Uji, Kyoto 611

As a part of a series of our investigations on the isotope effect upon the photodissociative excitation processes, relative emission cross sections of excited photofragment(s) formed by vacuum UV photolyses of $CHCl_3$ and $CDCl_3$ were determined. Figure 1(a) shows the emission excitation spectra of $CHCl_3$ and $CDCl_3$. The absorption spectrum of $CDCl_3$ is almost the same as that of $CHCl_3$ shown in Figure 1(b). The emission cross section for these two isotopic compounds are almost identical in the wavelength region above 122 nm, while below 120nm that for $CHCl_3$ is about a factor of 1.5 larger than that for $CDCl_3$. Two emitting species, CCl_2^* and $CHCl^*$, should be taken into account for the observed wavelength region. The observed isotope effect provides some more information about the emitting species. Below 120 nm, where isotope effect on emission cross section becomes apparent, CCl_2^* radical must be dominant because the CCl_2^* formation involves the C-H rupture whose rate is reduced by deuterium substitution. Above 120 nm where no isotope effect is observed, however, dominant emitting species must be $CHCl^*$ which is formed without C-H rupture. Consistently with this identification for emitting species, $CHCl^*$ radical is found to be dominant at 121.6 nm from lifetime measurements.

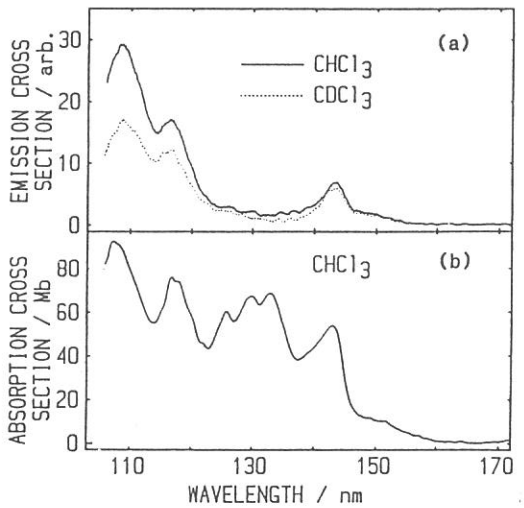

Figure 1. Emission excitation spectra of $CHCl_3$ and $CDCl_3$ (a), and absorption spectrum of $CHCl_3$ (b).

ABSORPTION AND FLUORESCENCE EXCITATION SPECTRA OF H_2O IN SUPERSONIC FREE JET

Atsunari HIRAYA and Kosuke SHOBATAKE

Institute for Molecular Science, Myodaiji, Okazaki, 444 Japan

Spectroscopic and photochemical investigations for the electronically excited molecules in the gas phase are often limited by thermal distrbutions of the vibrational and rotational levels. Such a limitation has been circumvented by using a supersonic free jet technique that provides rotationally and vibrationally cooled molecules in the gas phase. Furthermore, this technique has been known to be quite useful for producing many varieties of molecular clusters. However, for the jet-cooled molecules, only very few direct absorption spectra and emission excitation spectra have been observed in the VUV region. This is mainly due to some limitations, such as the wavelength region, tunability and stability of light soureces. These limitations can be overcome to a considerable extent by means of SOR as a light source, even though there are some disadvantages of SOR compared to lasers, i.e. wavelength resolution and intensity.

We report here preliminary results of the measurment of direct absorption and fluorescence excitation spectra of H_2O in a free jet. In the present measurement, the H_2O vapor at 250 torr was diluted with 1.5 atm He carrier gas and continuously expanded through an orifice (0.15 mm dia.) kept at 120°C into the main chamber pumped by a 10" difusion pump backed by a mechanical booster pump. Dispersed SOR light was focused on the

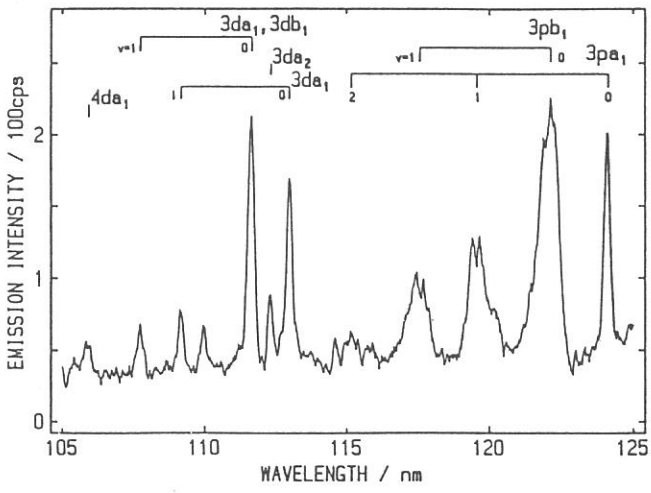

Figure 1. Emission excitation spectrum of H_2O cooled in free jet.

free jet and the emission from OH^* formed from the photo-dissociation of H_2O is recorded against excitation wavelength. An emission excitation spectrum of H_2O cooled in a continuously expanded free jet over 105 - 125 nm is shown in Figure 1. Almost all of the observed bands are Rydberg bands, already assigned as indicated in Figure 1. In order to examine the rotational cooling in the free jet, absorption and emission excitation spectra of room temperature vapor were also measured by filling low pressure H_2O vapor in the chamber without pumping. Figure 2 shows the absorption and emission excitation spectra obtained for room temperature vapor (upper) and for CW free jet (lower) conditions, where the wavelength resolution of light are 0.2 nm for both conditions. In the vapor, widths of 111.6 nm band in absorption and emission excitation spectra are 0.52 nm and 0.63nm, respectively, while those in the free jet is sharpened to 0.22 nm and 0.25 nm. It is quite evident that considerable cooling is attained by the CW free jet. It should be noted that the band widths and band shape of emission excitation spectra are different from those of absorption spectra for both conditions. This implies that the quantum yield for OH^* formation is strongly dependent on the rotational levels of the initially prepared Rydberg states.

It may be useful to give the detection limits for the absorption and emission band in a practical way as products $P \cdot \mu$ and $P \cdot \mu \cdot Q$, respectively, where P is sample pressure(torr) before expansion, μ is absorption coefficient given as absorption cross section σ(Mb = 10^{-18} cm^2) or molar extinction coefficient ε($dm^3 mol^{-1} cm^{-1}$) and Q(%) is emission quantum yield. For our present apparatus, these products should be

for absorption :

$$P \cdot \sigma > 10^4, \quad P \cdot \varepsilon > 3 \times 10^6$$

for emission :

$$P \cdot \sigma \cdot Q > 10^1, \quad P \cdot \varepsilon \cdot Q > 3 \times 10^3$$

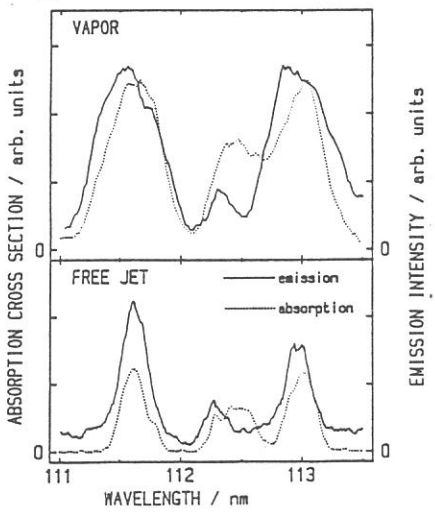

Figure 2. Absorption and emission excitation spectra of H_2O in room temperature vapor (upper) and in free jet (lower).

FLUORESCENCE LIFETIME MEASUREMENT FOR GAS PHASE MOLECULES EXCITED IN VUV REGION BY SYNCHROTRON RADIATION.

Atsunari HIRAYA and Kosuke SHOBATAKE

Institute for Molecular Science, Myodaiji, Okazaki, 444 Japan

The synchrotron radiation from UVSOR having pulse charactaristics of high repetition rate (90.1 or 5.63 MHz), short duration (ca. 400 ps) and stable intensity in the VUV - UV region, is a very useful light source for the studies of dynamics of highly excited states and photodissociative excitation processes. We reports the successfull installation of a time-resolved fluorescence measurement system in a gas phase fluorescence apparatus on a beam line BL2A. Figure 1 shows a block diagram for the time-resolved fluorescence measurement system.

As an example of the succcesful application of this system to the time-resolved measurements, the fluorescence decay curve of the CN^* radical formed by the photo-dissociation of CD_3CN vapor (50 mtorr) excited at 110 nm is shown in Figure 2. The time response of the scattered light is also shown for comparison. This measurement was performed when the machine was operated in a single bunch operation mode. Although the observed decay curve cannot be expressed exactly by a single exponential function, the lifetime of the fast decaying component is estimated to be about 80 ns. This value is in good agreement with the radiative lifetime (85 ns) of $CN^*(B-X)$.[1] It should be mentioned that a relatively high base-line (ca. 300counts) of the decay curve is mainly resulted from overlapping of successive slow decaying components whose lifetime is several times longer than the time interval of excitation light pulses. This slow decaying component should be due to the $CN^*(A)$ whose radiative lifetime to the ground state is known to be 4.2 μs.[1]

Reference

1) T. J. Cook and D. H. Levy, J. Chem. Phys., **57**, 5059 (1972); ibid. 57, 5050 (1972).

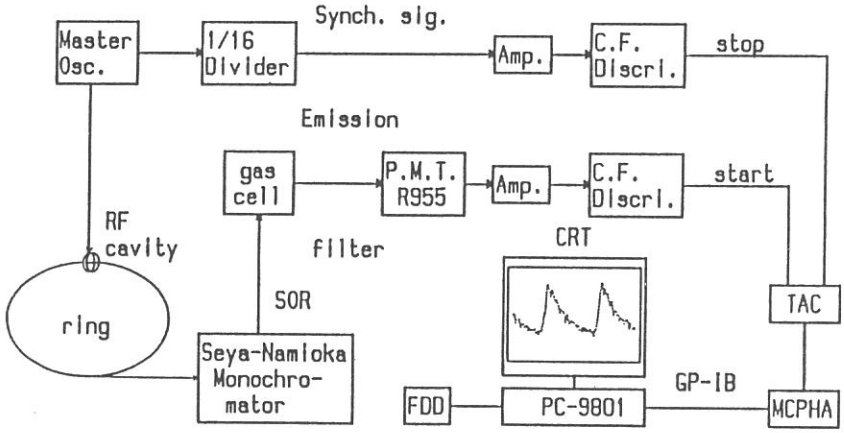

Figure 1. Block diagram for the time-resolved fluorescence measurement system installed in a beam line BL2A of UVSOR. TAC, time-to-amplitude converter; MCPHA, multichannel pulse-height analyzer.

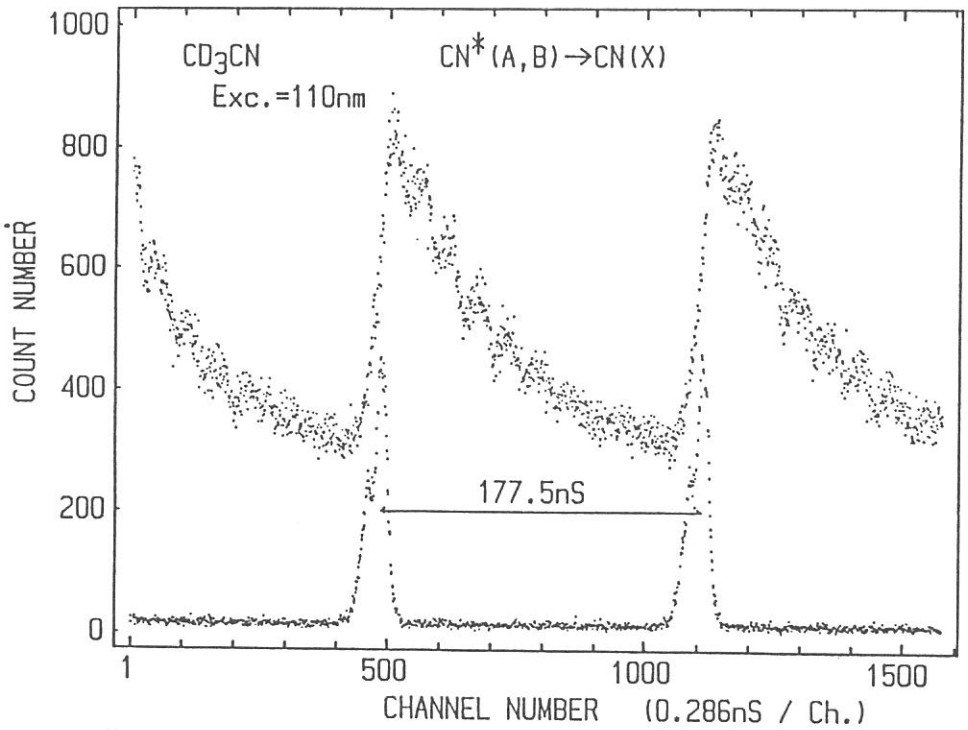

Figure 2. Decay curve of the emission observed from CD_3CN vapor (50 mtorr) after excitation at 110 nm (upper trace) and the time response for scattering light at 200 nm (lower trace).

Observation of the Threshold Energies of H^+ Formation Ethylene and Acetylene by Synchrotron Radiation. Determination of the C-H Bond Dissociation Energies.*

Haruo Shiromaru, Yohji Achiba**, Katsumi Kimura,
and Yuan T. Lee***
Institute for Molecular Science, Okazaki 444

The C-H bond dissociation energies of ethylene and acetylene, (D_0(R-H): R = C_2H_3, C_2H) are the important quantities to be accurately determined in chemistry. The D_0 values can be deduced from the relationship

$$D_0(R\text{-}H) = E_{th}(H^+) - I(H) \qquad (1)$$

where $E_{th}(H^+)$ is the threshold energy for the reaction

$$RH + h\nu = R + H^+ + e^- \qquad (2)$$

and I(H) is the ionization energy of the H atom (13.598 eV). In the present work, we have been able to determine D_0(R-H) values for the first time from the onset of photoionization efficiency curves.

Photoionization measurements were performed in the energy region 58 - 70 nm using the beam port BL2-B2 of UVSOR. Helium or argon gas was used as a filter to diminish the higher-order light. A sample gas was introduced as a molecular beam in order to avoid an ion molecular reaction. A Q-pole mass filter (ULVAC Model MSQ-400) was used for mass analysis and detection.

The H^+ efficiency curves obtained for ethylene and acetylene are shown in Figs. 1 and 2, respectively. The increasing backgrounds (indicated by solid lines) in Figs. 1 and 2 are due to the ionization by residual second-order radiation from the

* To be Published in J. Phys. Chem. (1987).

** Present address: Department of Chemistry, Tokyo Metropolitan Univ., Tokyo 158

*** On leave from Lawrence Berkeley Laboratory and the Department of Chemistry, University of California, CA 94720, as IMS visiting professor (March-June, 1986)

monochromator. The H^+ efficiency curves obtained at different pressures of the helium filter gas are compared in Fig. 1: (a) 0 Torr, (b) 0.050 Torr, (c) 0.098 Torr. The background signals seem not to affect the position of the onsets.

From the efficiency curves (Figs. 2 and 2), we have obtained

$E_{th}(H^+)$ = 18.66 eV, D_0 = 5.06 eV for ethylene

$E_{th}(H^+)$ = 19.35 eV, D_0 = 5.75 eV for acetylene

The D_0 values deduced here are in good agreement with these obtained from the analysis of the photofragment translational spectra but considerably higher than those derived from the onset of C_2H^+ or $C_2H_3^+$ using the relationship

$$D_0 = E_{th}(R^+) - I(R) \qquad (3)$$

The deviation may be due to the effect of ion pair formation.

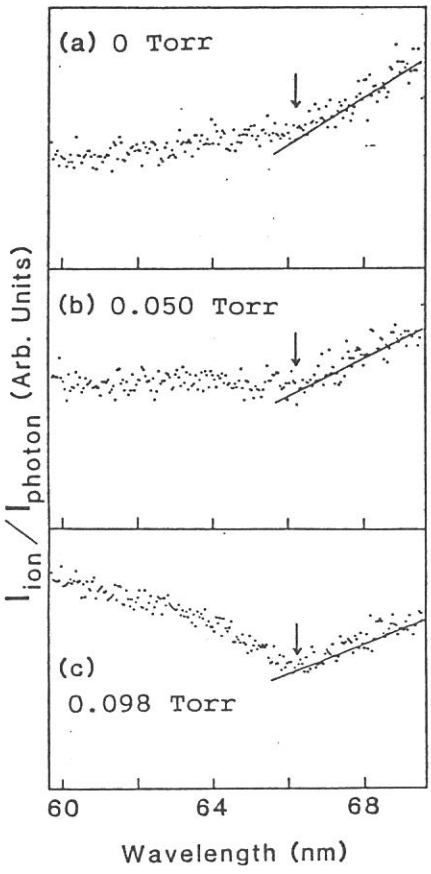

Fig. 1. The efficiency curves of H^+ for C_2H_4.

The synchrotron radiation is suitable for the determination of the C-H bond dissociation energies because of its high intensity and stability in the wavelength region relevant to the H^+ formation.

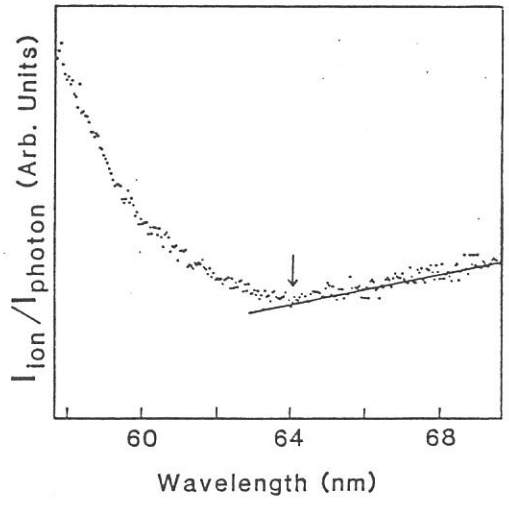

Fig. 2. The efficiency curves of H^+ for C_2H_2.

PHOTOIONIZATION MASS SPECTROMETRY OF DIMETHYLETHER AND CYCLOHEXANE

M. Ukai, S. Arai, T. Kamosaki, K. Hayashi, K. Shinsaka, and Y. Hatano.

Department of Chemistry, Tokyo Institute of Technology,
Meguro-ku, Tokyo 152.

H. Shiromaru and K. Kimura.

Institute for Molecular Science,
Myoudaiji, Okazaki-shi, Aichi 444.

Spectroscopy and dynamics of highly excited molecules produced by photon impact in extreme ultra violet region are of fundamental importance in understading the interaction of photons with molecules. Especially studies of chemically important molecules, such as hydrocarbons, alcohols, and ethers, are almost completely open field where importance of autoionization of highly excited molecules has been recognized.

The gross feature of the total photoabsorption cross sections and the ionization efficiencies near thresholds for C_3H_6, C_4H_8, C_6H_{12}, C_2H_6O, and C_3H_8O isomers have been determined by our previous works[1-3]. However, detailed information on the products has not been obtained extensively in a wide region of photon energy.

The present paper reports the photoionization mass spectra of dimethyl ether and cyclohexane obtained by using a quadrapole mass spectrometer in a wavelength region of 40-90nm of SR from BL-2B2 at UVSOR, IMS.

Mass fragment patterns of dimethyl ether are obtained at various photon energies. Intense peaks are observed at m/e=15, 29, 45, and 46 which, respectively, correspond to CH_3^+, CHO^+, $CH_3OCH_2^+$, and $CH_3OCH_3^+$. The peak of 45 is the most intense. The peak of 31 (CH_3O^+) is much weaker than that in the previous work[4]. Excitation spectra

for specific fragments are observed in which ionization onsets, peaks, and shoulders are observed (fig. 1). The gross maximum and the broad structures in the previous total absorption spectrum are explained by the respective structures in the present spectra. Characteristic vibrational structure which has been observed in the previous total absorption spectrum[2] are not observed in the present spectrum of 46.

Fragment patterns and excitation spectra are also obtained for cyclohexane.

References

1. H. Koizumi, T. Yoshimi, K. Shinsaka, M. Ukai, M. Morita, Y. Hatano, A. Yagishita, and K. Ito, J. Chem. Phys., 82, 4856 (1985).

2. H. Koizumi, K. Hironaka, K. Shinsaka, S. Arai, H. Nakazawa, A. Kimura, Y. Hatano, Y. Ito, Y. Zang, A. Yagishita, K. Ito, and K. Tanaka, J. Chem. Phys., 85, 4276 (1986).

3. H. Koizumi et al., J. Chem. Phys., (to be published).

4. R. Botter, J. M. Pechine, and H. M. Rosenstock, Int. J. Mass. Spectr. Ion. Phys., 25, 7 (1977).

Figure 1

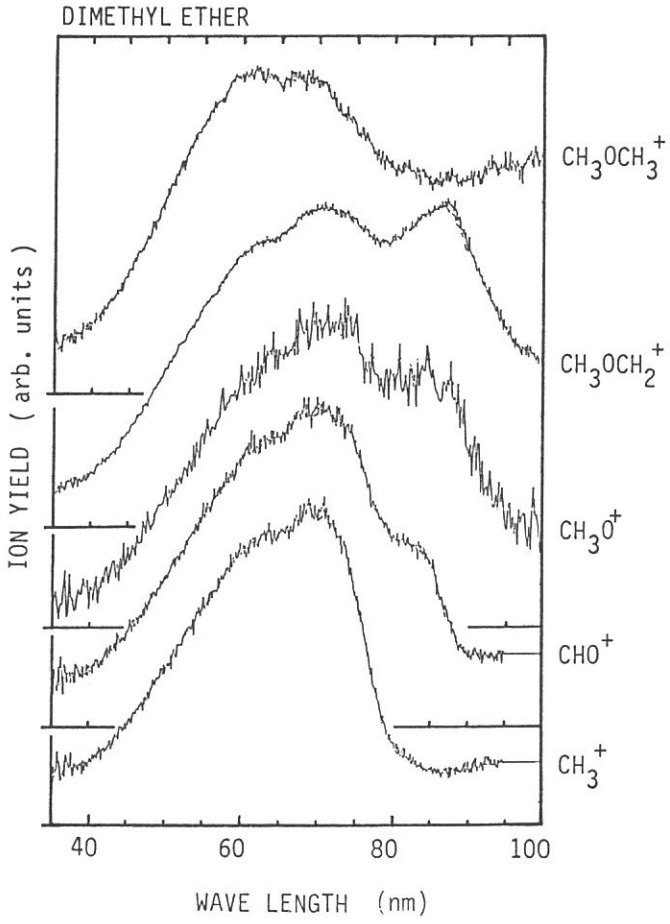

UVSOR STUDY OF CO_2-H_2O CLUSTERS

Hideyuki SUZUKI, Masahiro KAWASAKI, Hiroyasu SATO,
Haruo SHIROMARU* and Katsumi KIMURA*

Chemistry Department of Resources, Faculty of Engineering,
Mi'e University, Tsu 514
* Institute for Molecular Science, Myodaiji, Okazaki 444

CO_2-H_2O clusters formed under molecular-beam conditions by seeding H_2O in CO_2 gas were photo-ionized in the BL2B2 molecular beam photoionization spectrophotometer, and the resulting cluster ions were analysed by a quadrupole mass analyser. The diameter of the nozzle was 50 μm, that of the skimmer was 0.7 mm, and the distance of the nozzle and skimmer was set at 3 mm. The stagnation pressure was adjusted by mixing H_2O at the vapor pressure of the room temperature with CO_2 at various pressures. The sample gas was injected continuously through the nozzle.

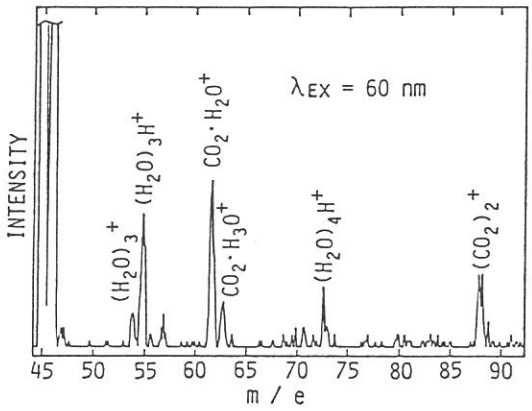

Fig. 1. Mass spectrum at a stagnation pressure of 3.9 atm.

The mass spectrum observed at the stagnation pressure of 3.9 atm. is shown in Fig. 1. The signals at the m/e values 54, 55, 62, 63, 73 and 88 can be asigned to $(H_2O)_3^+$, $(H_2O)_3H^+$, $CO_2 \cdot H_2O^+$, $CO_2 \cdot H_3O^+$, $(H_2O)_4H^+$, and $(CO_2)_2^+$, respectively.

The photoionization efficiency curve for m/e=62 ($CO_2 \cdot H_2O^+$) is given in Fig. 2. Broad humps at 76 nm and

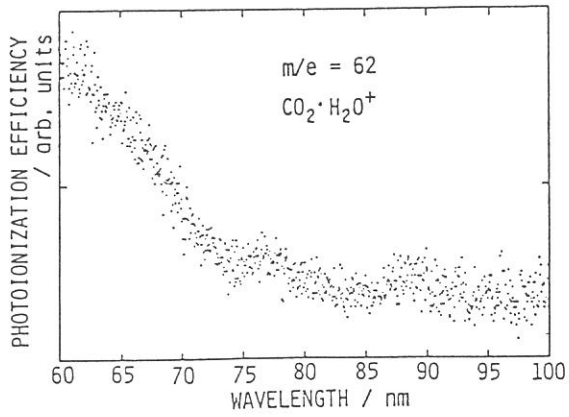

Fig. 2. Photoionization efficiency curve for m/e=62 ($CO_2 \cdot H_2O^+$).

88 nm may be due to the photoionization of the CO_2 moiety.

The photoionization efficiency curves for m/e=62 ($CO_2 H_2O^+$), 44 (CO_2^+), 18 (H_2O^+), and 19 (H_3O^+) are shown in Fig. 3. The curve of $CO_2.H_2O^+$ (Fig. 3a) differs in shape from CO_2^+ (Fig. 3b) or H_2O^+ (Fig. 3c); the photoionization efficiency increases fairly steeply to the shorter wavelength from ca. 74 nm. The appearance of $CO_2.H_2O^+$ (Fig. 3a) is close to that of H_3O^+ (Fig. 3d) which is considered to be formed from $(H_2O)_n$. The photoionization efficiency curve of m/e=63 ($CO_2.H_3O^+$) was also measured (not shown); its shape was similar to that of m/e=62 ($CO_2.H_2O^+$). These findings suggest that the observed intensity for m/e=62 ($CO_2.H_2O^+$) is due to the fragmentation of $Co_2.(H_2O)_n$, and this contribution causes the rise from ca. 74 nm. A similar situation occurs for the efficiency curve of H_3O^+.

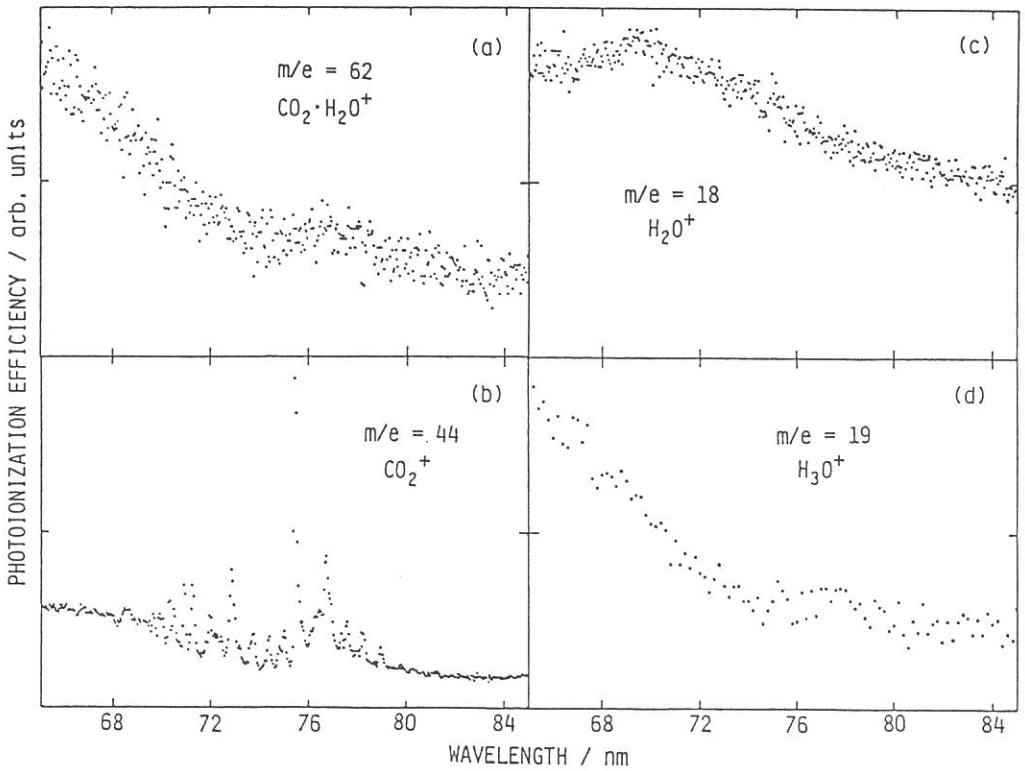

Fig. 3. Photoionization efficiency curve for (a) m/e=62 ($CO_2 \cdot H_2O^+$), (b) m/e=44 (CO_2^+), (c) m/e=18 (H_2O^+), (d) m/e=19 (H_3O^+).

THRESHOLD ELECTRON SPECTRA OF SOME DIATOMIC MOLECULES FOR THE STUDY OF STATE SELECTED ION-MOLECULE REACTIONS

Shinzo SUZUKI and Inosuke KOYANO

Institute for Molecular Science, Myodaiji, Okazaki 444

The TEPSICO-II apparatus[1] has been installed at BL3B for the study of state-selected unimolecular and bimolecular reactions of ions using synchrotron radiation. With this apparatus it is possible to utilize the TESICO (threshold electron-secondary ion coincidence) technique[2] to select internal states or internal energies of reactant ions. For the TESICO experiments, it is necessary to know threshold electron spectra (TES) of parent molecules for the reactant ions and see what electronic or vibrational states exist in the wavelength region of interest. Synchrotron radiation is a suitable continuum VUV light source for such experiments.

Fig. 1 shows the TES of O_2 in the wavelength range 63-83 nm taken with the TEPSICO-II apparatus. The gross features agree well with those of Guyon and Nenner.[3] A series of peaks appears in the so-called Franck-Condon gap (the region 95.3 - 77.5 nm) where there is no direct ionization probability. This demonstrates the advantage of the TESICO technique for the study of state-selected reactions.

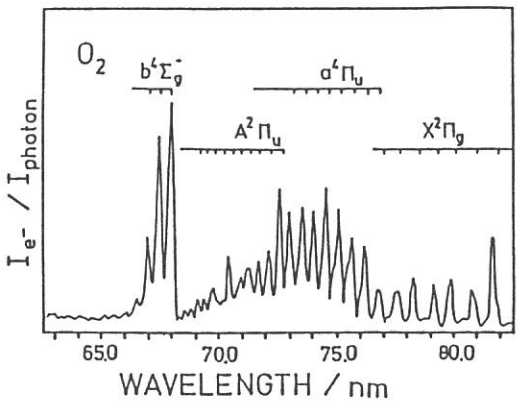

Fig. 1 Threshold electron spectrum of O_2

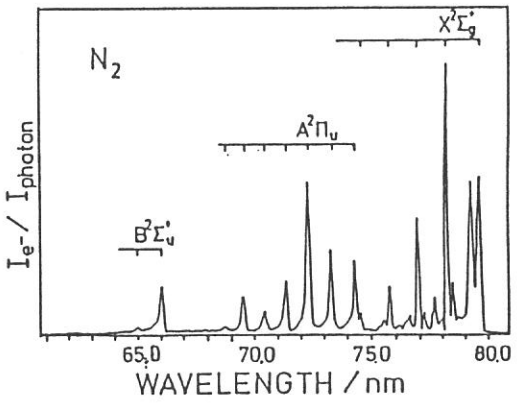

Fig. 2 Threshold electron spectrum of N_2

The TES of N_2 is shown in Fig. 2. It indicates that the reactions of $N_2^+(X)$ can be studied up to v = 4, while in the HeI photoelectron spectrum of N_2, $N_2^+(X)$ ions produced are dominated by v = 0, with small fraction of v = 1. The discrepancy between this and the Peatman et al.[4] spectrum concerning the peaks around the v = 0 and 1 thresholds is due to the difference in the resolution of the two electron energy analyzers.

Fig. 3 shows the TES of NO in the wavelength range 50.0 - 80.0 nm. The TES in the 50.0 - 60.0 nm range is reported here for the first time and shows a single peak at 57 nm, which is assigned in comparison with an ESCA spectrum [5] to $^3\Pi$ state resulting from removal of an 4σ electron. The occurrence of these threshold electrons suggests the possibility of studying processes following the inner valence excitation.

References

1. I. Koyano, K. Tanaka, T. Kato, S. Suzuki and E. Ishiguro, Nucl. Instr. Meth., A246 (1986) 507.
2. I. Koyano and K. Tanaka, J. Chem. Phys., 72 (1980) 4858.
3. P. M. Guyon and I. Nenner, Appl. Opt. 19 (1980) 4068.
4. W. B. Peatman, B. Gotchev, P. Gurtler, E. E. Koch and V. Saile, J. Chem. Phys. 69 (1978) 2089.
5. ESCA applied to free molecules. K. Siegbahn, C. Nordling, G. Johansson, J. Hedman, P. F. Heden, K. Hamrin, U. Gelius, T. Bergmark, L. O. Werme, R. Manne, Y. Baer (eds.), p.74. Amsterdam: North-Holland 1969.

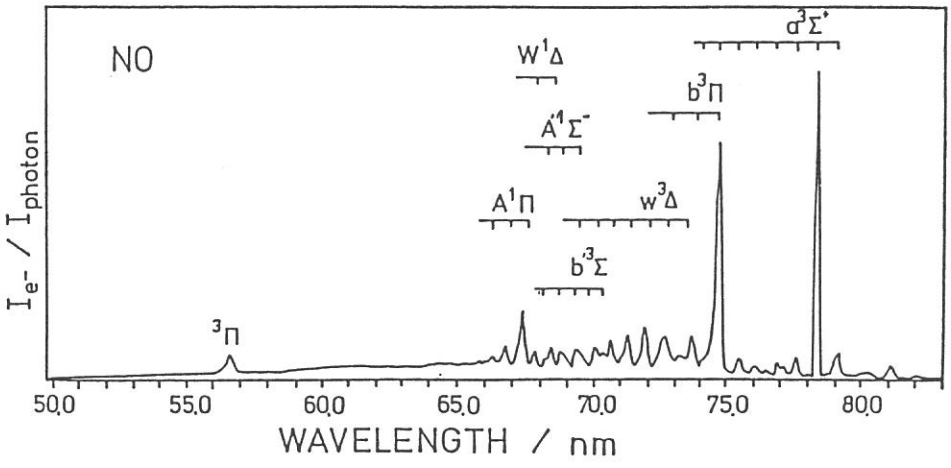

Fig. 3 Threshold electron spectrum of NO

Dissociation mechanism of state selected NO_2^+ ions

Kazuhiko SHIBUYA*, Shinzo SUZUKI, and Inosuke KOYANO

Institute for Molecular Science, Myodaiji, Okazaki 444
*Department of Chemistry, Tokyo Institute of Technology, Ohokayama, Tokyo 152

The equilibrium geometries of NO_2 molecules and NO_2^+ ions are quite different in their ground electronic states. This has long been baffle for the accurate determination of adiabatic ionization potential of NO_2. On the other hand, the ejection of an inner valence electron from NO_2 is Franck-Condon allowed due to their similar geometries. Therefore, one can prepare electronically excited and state selected NO_2^+ ions by a photoionization method in the spectral region shorter than 100 nm. For the purpose of elucidating the dissociation mechanism of state selected NO_2^+ ions, we have measured the threshold electron spectrum (TES) of NO_2, the photoionization efficiency (PIE) curves for its parent and fragment ions, and the threshold electron - ion TOF coincidence spectra in the range 40 - 80 nm using TEPSICO-II.

Fig.1 shows TES of NO_2, which accords well with the He I photoelectron spectrum of NO_2 [1]. In this region triplet states are mainly observed, $^3B_2(2b_2)^{-1}$ and $^1B_2(2b_2)^{-1}$ making a pair of $(2b_2)^{-1}$ ionization.

Fig.2 shows photoionization efficiency curves for the fragment (O^+,NO^+) and parent (NO_2^+) ions. The O^+ production was observed in the region shorter than 65 nm, which accords with the location of $^3B_2$. Fig.3 shows the TOF coincidence spectra obtained with excitation at 65.4 nm, corresponding to the onset of $^3B_2$ v_1=0. The O^+/NO^+ branching ratio was obtained to be 0.66. The vibrational dependence of the ratio was not observed within the $^3B_2$ state to an appreciable extent.

From similar measurements at 57.9 nm (formation of $^1B_2$ and/or $^3A_1$), the ratio of O^+/NO^+ was found to be 0.16, which is four times as small as the ratio derived for $^3B_2$. Possibly, the fragmentation pattern of excited NO_2^+ could be quite different depending on whether the relevant surface is singlet

or triplet.

Finally, we have observed NO_2^+ as a product with excitation around 71 nm, which prepares the parent ion in the $^3A_1$ and/or $^3B_1$ states lying approximately 5 eV above the dissociation limit. The $^3A_1$ and/or $^3B_1$ states are likely to be stabilized through radiative relaxation onto the $^3B_2$ and/or $^3A_2$ states.

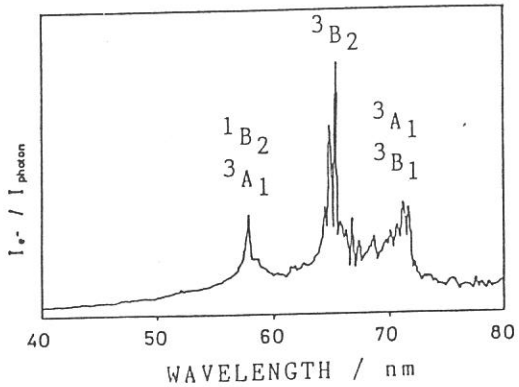

Fig. 1 TES of NO_2

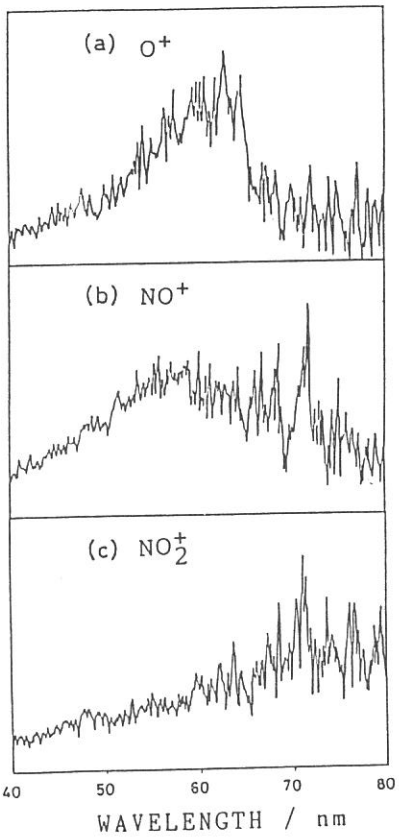

Fig. 2 PIE curves for parent and fragment ions

[1] C.R.Brundle et al.
J. Chem. Phys. 53, 705 (1970)

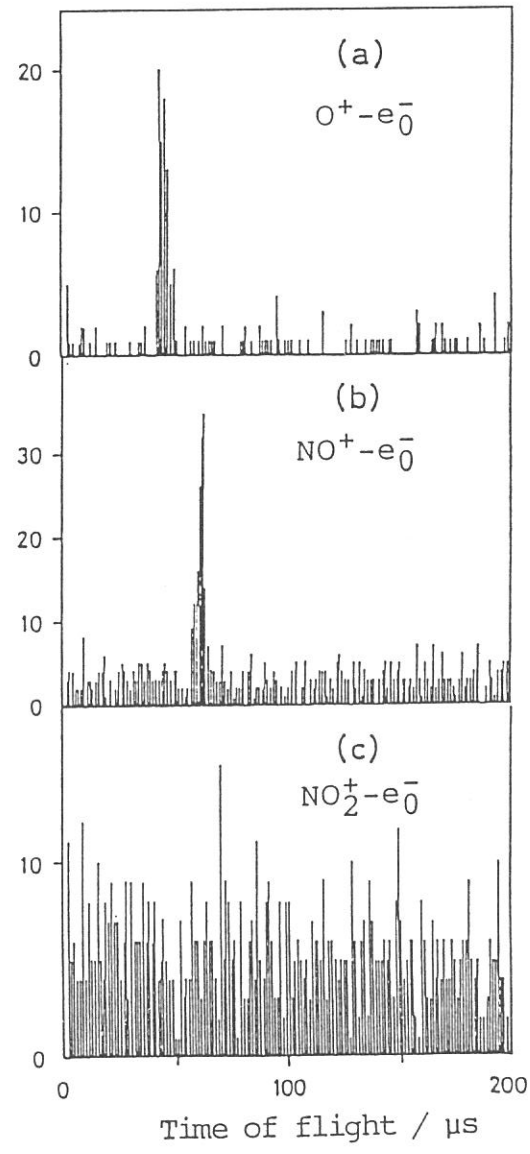

Fig. 3 TOF coincidence spectra obtained at 65.4 nm

INVESTIGATION OF FRAGMENTATION PROCESSES FOLLOWING CORE PHOTOIONIZATION OF ORGANOMETALIC MOLECULES IN THE VAPOR PHASE

Shin-ichi NAGAOKA, Shinzo SUZUKI and Inosuke KOYANO

Institute for Molecular Science, Myodaiji, Okazaki 444

Fragmentation processes following core photoionization of molecules are forming a research field of current interest. Volatile compounds with group II–V elements are particularly suitable for detailed investigations of these processes in the vapor phase, because the rather small binding energies of the (n-1)d core electrons allow the studies in the normal incidence region of the vacuum ultraviolet. Accordingly, we have attempted to study the core photoionization and subsequent fragmentation of such compounds ($Zn(CH_3)_2$, $Ga(CH_3)_3$, $Ge(CH_3)_4$, $Sn(CH_3)_4$, $Pb(CH_3)_4$, and $Bi(CH_3)_3$). Here, we report production of Pb^+ ion following Pb 5d core photoionization of tetramethyllead (TML) as revealed by using the threshold electron – photoion coincidence (TEPICO) method. The experiments were performed using the TEPSICO-II apparatus installed in BL3B beam line of UVSOR.

Figure 1 shows the threshold electron spectrum of TML. Several sharp bands seen in the region 44 – 75 nm are assigned to the photoionization from the Pb 5d core levels. Figure 2 shows the photoionization efficiency curves for fragment ions from TML. The photoionization efficiency curve for the Pb^+ ion has an appearance quite different from those for other fragments. Moreover, almost all peaks of the Pb^+ curve in the region 44 – 75 nm are found to coincide in position with those in the threshold electron spectrum of TML. Figure 3 shows an example of the time-of-flight coincidence spectrum. It is seen that sufficiently high signal-to-noise ratio is attained with reasonable data collecting time. Relative efficiency for the production of each fragment from various states of the TML parent ion were determined by use of TEPICO, and are given in Fig. 4. From these results, it is considered that the Pb^+ ion is predominantly produced following Pb 5d core photoionization.

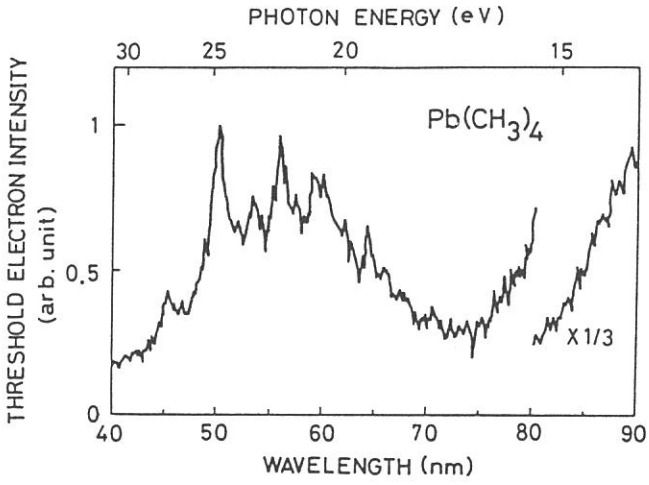

↑Fig. 1. Threshold electron spectrum of TML.

Fig. 2. Photoion efficiency curves for → fragment ions from TML.

↓Fig. 3. Time-of-flight TEPICO spectrum of the Pb^+ ion taken by excitation at 50.4 nm. Data collection time is 100 minutes.

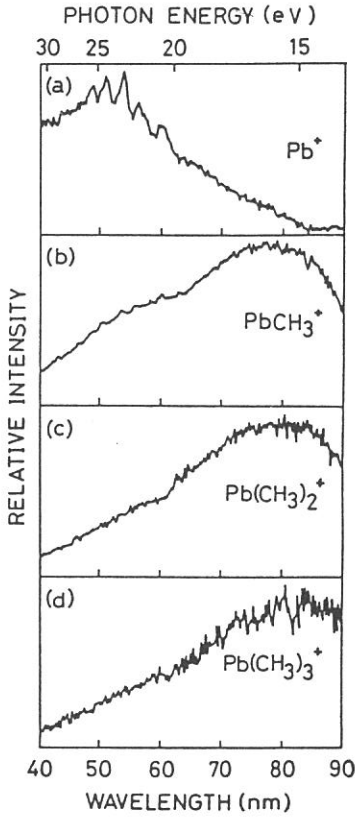

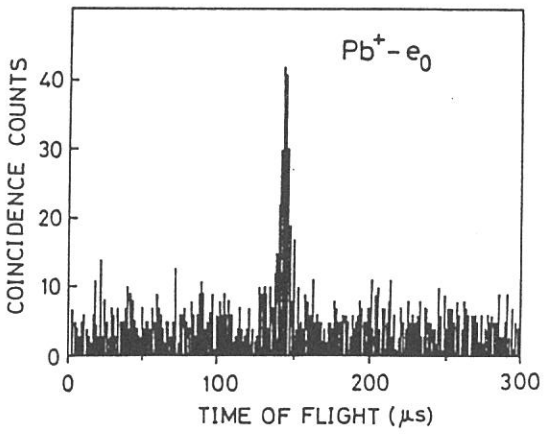

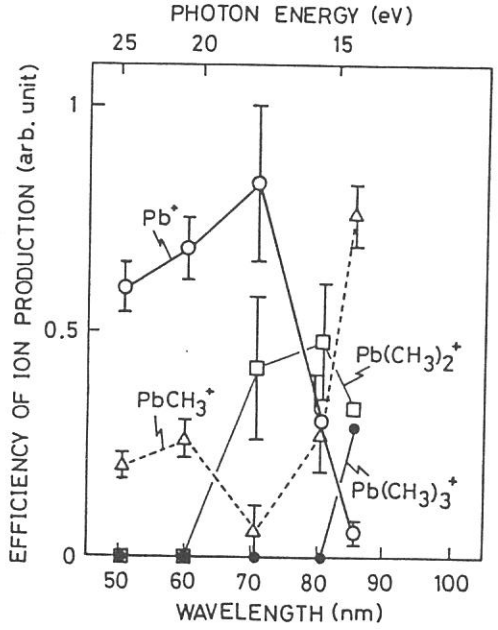

↑Fig. 4. State selected efficiency of ion production.

FORMATION OF H^- BY ELECTRON TRANSFER FROM Cs ATOMS TO H_2^+: DEPENDENCE ON THE VIBRATIONAL LEVEL OF H_2^+

Sigeo HAYAKAWA, Shinzo SUZUKI*, Masatugu KOGO, Toshio SUGIURA and Inosuke KOYANO*

The College of Integrated Arts and Sciences, University of Osaka Prefecture, Mozu-Umemachi 4-804, Sakai, Osaka 591
*Institute for Molecular Science, Myodaiji, Okazaki 444

This work is in progress, so that this report describe the development of the experiment and the interim results.

A large amount of work on the electron transfer for H^+ (or D^+) ions in metal vapour has been reported, from the viewpoint of neutral beam injection schemes in controlled thermonuclear fusion research. The study of the electron transfer processes with molecular ions, however, has not been published so far. Three of the present authors (Univ. Osaka Prefecture group) have obtained new information about the following successive electron transfer processes:

$$H_2^+ + Cs \longrightarrow H_2^* + Cs^+ \qquad (1)$$

$$H_2^* \longrightarrow 2H \qquad (2)$$

$$H + Cs \longrightarrow H^- + Cs^+ \qquad (3)$$

The formation cross section of H^- ions in these processes is over 2 times larger than that of H^- ion formation from H^+ ions. The H^- ions having various kinetic energies are formed, about a half of H^- ions formed having kinetic energy of 4.1 eV, and the other half having kinetic energies of 0.24 — 0.41 eV.

The purpose of the present experiment was to elucidate the dependence of process (1) on the vibrational level of the H_2^+ ions, using the coincidence measurements of product signals with threshold electrons. For this purpose, the photoionization chamber, reaction regions, and lens system of the TEPSICO-II apparatus[1] have been replaced with those shown in Fig. 1. An electron gun has been installed temporarily on the photo-ionization chamber, to examine the sensitivity of the detection system for the negative ions, using H^- ions formed in an ion pair process by electron impact.

A cylindrical Cs reservoir of 10 mm inner diameter and 50 mm long was made of stainless-steel. Chromel-alumel thermo-couples were attached to the target chamber, connecting tube, and Cs reservoir. These parts were heated separately by the nichrome wire insulated by glass sleeve. Cs vapour was fed to the target chamber by breaking in vacuum a glass ampule (containing 1g of Cs) put in the Cs reservoir. Cs density in the target chamber was estimated from available vapour pressure data.

Using this system, the following measurements have been made up to now: 1) photoionization efficiency curve and threshold electron spectrum of H_2, 2) time-of-flight coincidence spectrum of H_2^+ (v=0) ions as shown in Fig. 2, 3) the product spectrum of processes (1) to (3). The experiment 3) was performed under the condition that the impact energy of H_2^+ ions is 70 eV in the laboratory system and the Cs vapour density is 10^{14} atoms cm^{-3}. Under this condition, signals were obtained which were not affected by the potentials on the electrodes located downstream of the target chamber. These signals may be due to photons emitted from excited hydrogen atoms formed by dissociation process (2), or long-lived metastable excited hydrogen atoms. These signals would be distinguished by the measurement of the time of flight coincidence spectrum.

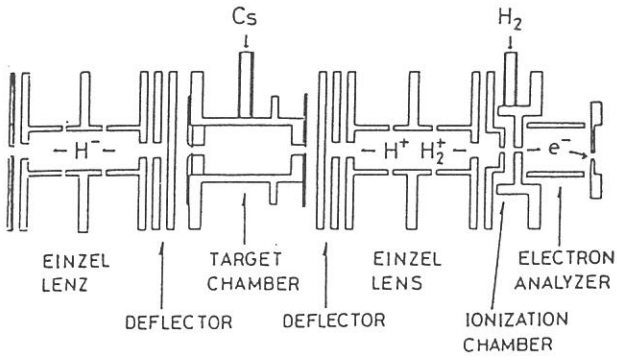

Fig.1 ionization and reaction region

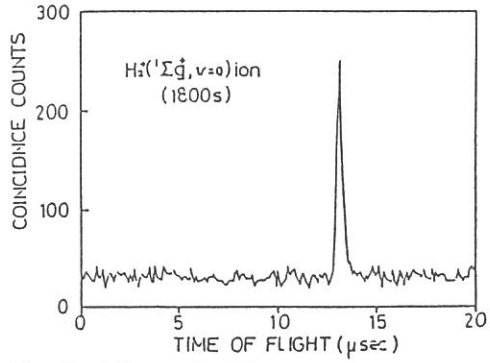

Fig.2. Time-of-flight coincidence spectrum of the H_2^+(v=0) ions

1) S. Suzuki et al., Z. Phys. D-Atoms, Molecules and Clusters 4, 111 (1986)

POLARIZED REFLECTION SPECTRA OF CADMIUM HALIDE CRYSTALS

Masami FUJITA, Hideyuki NAKAGAWA*, Yukio SHIMAMOTO*, Hiroaki MATSUMOTO*, Takeshi MIYANAGA**, Kazutoshi FUKUI*** and Makoto WATANABE***

Maritime Safety Academy, Wakaba, Kure 737
* Department of Electronics, Fukui University, Bunkyo, Fukui 910
** Department of Physics, Faculty of Education, Wakayama University, Sakaedani, Wakayama 640
*** Institute for Molecular Science, Myodaiji, Okazaki 444

Reflection spectra of single crystals of cadmium halides were measured by using synchrotron radiation of UVSOR. Light from strage ring was monochromatized with a plane grating monochromator at BL6A or a Seya-Namioka type monochromator at BL7B. Cleaved surfaces of single crystals were used for measurement.

In Fig. 1 are shown reflection spectra of $CdCl_2$, $CdBr_2$ and CdI_2 for polarization nearly perpendicular to the crystal c-axis ($E \perp c$) at liquid helium temperature. The spectra in the region below 10 eV agree with those measured with ordinary light sources.[1,2] Spectra obtained by Pollini et al. with SR[3] differ very much from present results.

The observed structures of three compounds can be classified into several groups. The peaks X, X_1 and X_2 around absorption edge are assigned to excitonic transitions from halogen p upper valence band to the lowest conduction band of Cd 5s character.[2] Sharp peaks A, B, B' and C are believed to be due to excitonic transitions in the deep interband energy region. A dip is observed at about 2 eV above the peak B. Beyond the dip appear peaks a – f. On going from chloride to iodide, the peaks a and b become distinct. Spin-orbit interaction of valence band may be responsible for the enhancement of the structure. Energy shift of the peaks d, e and f between chloride and iodide is somewhat smaller than that of a, b and c, which suggests that valence or conduction band relevant to the set of d, e and f is not the same as that of a, b and c.

The systematic variation in the spectral shape among three compounds suggests that the energy bands have the same ordering in each materials. From comparison of the spectra with band calculations,[3,4] set of peaks A, B, B' and C and that of a, b and c are assigned to transitions from upper valence band to Cd $5p_z$ and $5p_{x,y}$ conduction bands, respectively.

The peaks d, e and f are supposed to be associated with transitions from halogen p lower valence band.

In the region around 16 eV denoted by N are observed two (CdI_2 and $CdBr_2$) or three ($CdCl_2$) peaks. They are assigned to Cd 4d core excitons. The peaks are accompanied with several fine structures. Remarkable dichroic nature was revealed by preliminary measurement of the spectra for polarization parallel to the crystal c-axis (E // c). Crystal field at cadmium ion site is of D_{3d} symmetry. If optical excitation from $4d^{10}$ to $4d^9 5p$ of Cd^{2+} ion in the crystal field is assumed, 20 and 10 exciton states are allowed for E ⊥ c and E // c, respectively. Observed multiplicity and dichroism in the region N indicate that crystal field is essential to explain the Cd 4d core exciton states.

References

1) D. L. Greenaway and R. Nitsche: J. Phys. Chem. Solids 26 (1965) 1445.
2) S. Kondo and H. Matsumoto: J. Phys. Soc. Jpn. 51 (1982) 1441.
3) I. Pollini, J. Thomas, R. Coehoorn and C. Haas: Phys. Rev. B 33 (1986) 5747.
4) R. Coehoorn, G. A. Sawatzky, C. Haas and R. A. de Groot: Phys. Rev. B 31 (1985) 6739.

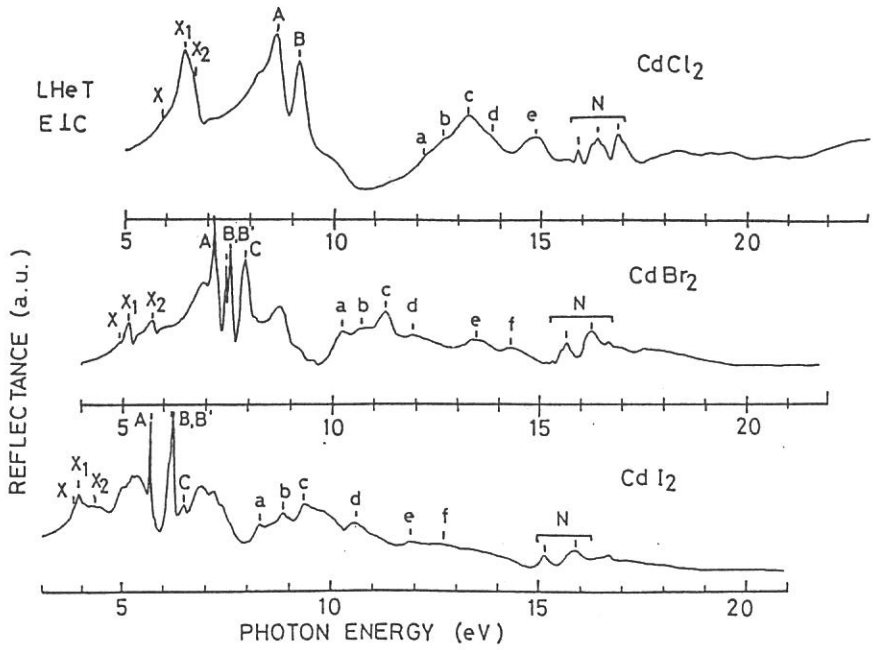

Fig. 1 Reflection spectra of cadmium halide single crystals at liquid helium temperature.

Polarized Reflection Spectra of Orthorhombic Indium Halides in 2 - 30 eV Region

Kaizo NAKAMURA, Yasuo SASAKI, Toru KISHIGAMI, Makoto WATANABE* and Masami FUJITA+

Department of Physics, Kyoto University, Kyoto 606
*Institute for Molecular Science, Okazaki 444
+Maritime Safety Academy, Kure 737

Polarized reflection spectra of orthorhombic indium halides (InBr and InI: space group D_{2h}^{17}) have been investigated at liquid helium temperature by using PGM spectrometer at BL6A2 in 2 - 30 eV region. Single crystals of InBr and InI were grown by Bridgman method. Results on InBr were reported previously.[1] In this report, results on InI are mainly described.

Figure 1 shows the spectra of InI for polarization parallel to the c-axis (E//c) and for E//a. The first exciton peak at 2.03 eV is due to the transition from the top valence band of iodine 5p, into which considerable amount of In 5s orbital admixes, to In 5p conduction band bottom. This transition is allowed for E//c. Many peaks are observed from 2 to 15 eV. They are attributed to the transition from the upper valence bands of I^- 5p and In^+ 5s to the lower conduction bands. At about 20 eV, In^+ 4d core exciton peaks are observed as in InBr.[1]

In Fig. 2, spectral features between 2 and 10 eV in both materials are compared with the energy shift of 0.85 eV. Many peaks coincide in energy suggesting that these transitions occur in In sublattice, that is, In 5s valence band (the second one) to In 5p conduction band.

Fig. 3 shows the spectra of In 4d core excitons in InI in an expanded energy scale. Spectra are very dichroic. Each of two main peaks, which have been observed in InBr with the separation of 0.8 eV, splits clearly in InI into two or more peaks. In the previous report, 4d exciton structure in InBr was explained by the atomic model without including the effect of crystal field.[1] To understand this dichroism and splitting, however, analysis

including crystal field as well as spin-orbit and exchange interactions has been attempted. It is found that the crystal field splitting amounts to 1 eV and is comparable to that of spin-orbit interaction.

1) K. Nakamura, Y. Sasaki, M. Watanabe, and M. Fujita: to be published in Physica Scripta 35 (1987).

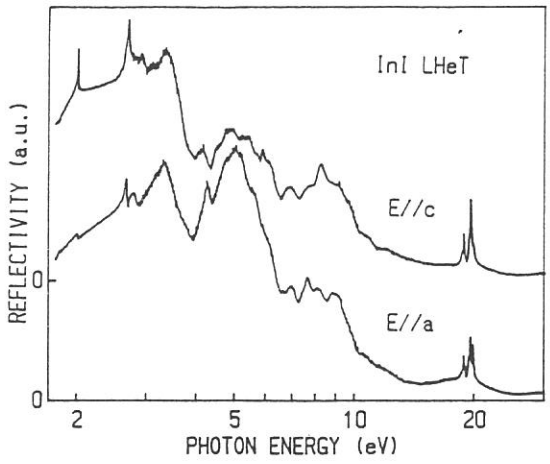

Fig. 1. Reflection spectra of InI at liquid helium temperature. (a) for E//c and (b) for E//a.

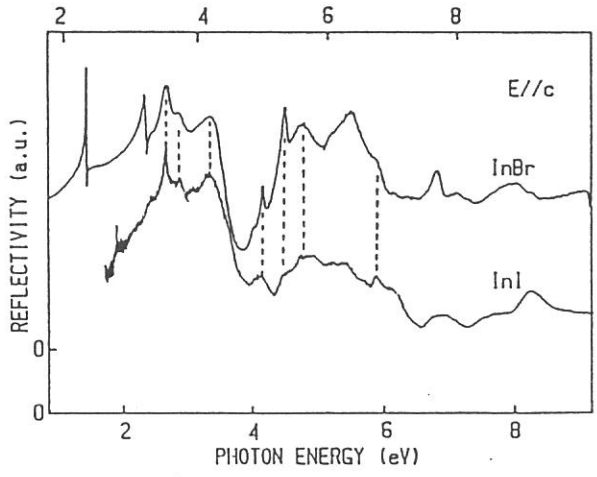

Fig. 2. Spectra of InBr and InI at LHeT for E//c from 2 to 10 eV. Energy for InI is shifted to higher energy by 0.85 eV.

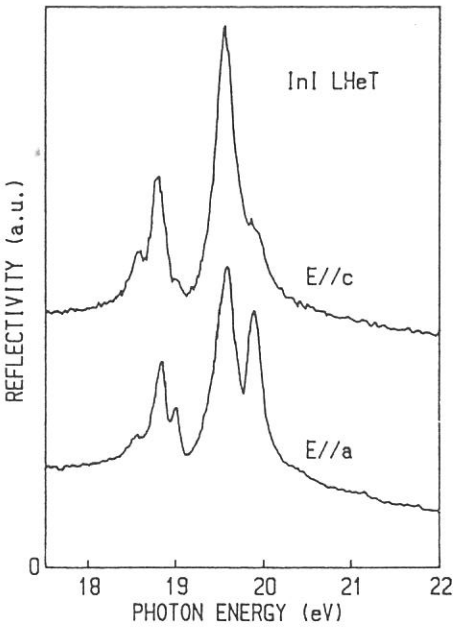

Fig. 3. Reflection spectra of 4d core excitons in InI at LHeT.

Absorption Spectra of SnTe Thin Films in 2-120 eV Region

Kazutoshi FUKUI, Jun-ichiro YAMAZAKI, Eiken NAKAMURA, Osamu MATSUDO,
Tadaaki SAITO*, Shin-ichi KONDO* and Makoto WATANABE

Institute for Molecular Science, Okazaki 444
*Department of Applied Physics, Fukui University, Fukui 910

SnTe films are known to be amorphous when evaporated onto substrates held at near liquid nitrogen temperature (LNT).[1] As the temperature goes up from LNT, irreversible amorphous-crystalline transformation occurs at the temperature T_c of about 200 K.[2] At T_c, the insulator-metal transition happens, that is, the resistivity shows an abrupt decrease from the order of 10^2 ohm.cm (amorphous phase) to 10^{-4} ohm.cm (crystalline phase). In this experiment, the effect of amorphous-crystalline transformation on optical spectra was investigated.

The substrates were thin collodion films. The in-situ measurements on SnTe films of both phases were carried out in 2 - 120 eV energy range by using a plane grating monochromator (PGM) at BL6A2. At the first time, SnTe film was evaporated on the substrate cooled to about 80 K under a vacuum of about 10^{-9}-10^{-10} Torr and the absorption measurement was carried out. Secondly, the film was annealed at room temperature and after that it was cooled to about 80 K, and the measurement was made again.

Figure 1 shows the absorption spectra of SnTe film of amorphous phase and crystalline phase at about 80 K. The structure below 26 eV is due to the transitions from valence band. Below 26 eV, a few broad peaks are observed in amorphous phase, and several peaks appear after crystallization. Below 6 eV, this result is consistent with the previous measurement.[3] The structure for crystallized SnTe below 20 eV is in good agreement with previous results.[4] The structure above 26 eV is due to the transition from core levels. Doublet structures around 26 eV are due to the transition from Sn 4d core level. They are likely to be due to the excitonic transition because the peaks are sharp. A structure around 44 eV is due to the transition from Te 4d core level. As the structure is broad, it does not seem to be due to the excitonic transition in contrast with the transition from Sn 4d core level. The electron-hole interaction for the transition from Sn 4d is larger than that from Te 4d. It may be related with the fact that the bottom of the conduction band consists

mainly of Sn 5p. (The top of the valence band consists mainly of Te 5p.) After crystallization, the peaks around 26 eV become sharper and several broad peaks appear above 50 eV.

In the MgBi alloy system, the insulator-metal transition occurs at the critical composition. In the core absorption spectra of this system, the excitonic shape of the first and the second peaks in the insulator phase (amorphous) became broad in the metal phase (crystalline).[5] This is attributed to the difference of screening effect, in which the difference of the conductivity is taken into account. In our system, however, we could not find such change in the line shape at the insulator-metal transition.

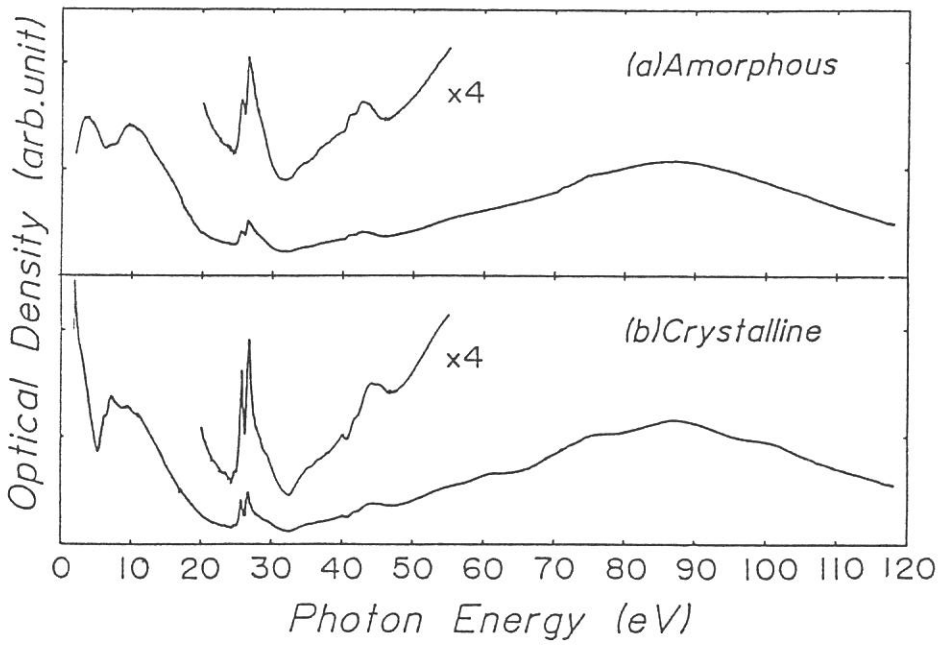

Figure.1. Absorption spectra of SnTe film at about 80 K.
(a) for amorpnous phase and (b) for crystalline phase.

REFERENCES

1) R.W.Brown,A.R.Millner and R.S.Allgaier:Thin Solid Films 5 (1970) 157.
2) K.Fukui,K.Inoguchi,S.Kondo and T.Tatsukawa:Jpn. J. Appl. Phys. 23 (1984) 1141.
3) M.Yoshikawa:Master Thesis (Fukui Univ. 1985)
4) M.Cardona and D.L.Greenaway:Phys. Rev. 133 (1964) A1685.
5) J.H.Slowik:Phys. Rev. B 10 (1974) 416.

K-Edge Absorption Spectra of Na and Mg Halides

Takatoshi MURATA, Tokuo MATSUKAWA*, Masaki OBASHI*, Shunichi NAO-E**, Hikaru TERAUCHI***, and Yasuo NISHIHATA***

Department of Physics, Kyoto University of Education, Fushimi-ku, Kyoto 612
*Department of Physics, College of General Education, Osaka University, Machikaneyama, Toyonaka 560
**Department of Physics, College of General Education, Kanazawa University, Kanazawa 920
***Department of Physics, Faculty of Science, Kwansei-Gakuin University, Nishinomiya 662

K-edge absorption specta of Na and Mg halides were measured at BL-7A soft x-ray beam line by using double crystal monochromator (DXM)[1]. Flat beryls were used as monochromator crystals.

Samples of NaF, NaCl, NaBr and MgF_2, $MgCl_2$, $MgBr_2$ were evaporated in situ onto collodion film deposited on Ni fine mesh. All the measurements were made at room temperature. We believe that this is the first measurement for the Mg K absorption in magnesium halides.

In Figs. 1 and 2 are shown the cation K-edge absorption spectra of NaCl and $MgCl_2$. In both spectra are observed a very sharp absorption bands at the lowest energy. Another intersting point is the appearance of a small hump at the lower edge of the sharp band in both spectra. This small hump is observed in all the spectra of other measured materials.

For the assingnment of the structure of the spectra, we classify the structure into two groups; above mentioned two peaks, and other structures beyond them. The first group may be attributed to the excitonic transition of the 1s core electron. The sharp band can be interpreted as core excitons arising from 1s-3p transitions in Na^+ or Mg^+ ions. The origin of the hump is not clear at the moment, but we tentatively assign the structure as a forbidden transition from 1s to 3s state in metal ions.

The structure at the higher energy side of the first peak is also very sharp in both materials, but the separation between the peaks are dependent upon the materials. Positions of peaks beyond them are also material depen-

dent. Therefore, these structure may be attributed to the transition to the final state due to multiple scattering of the excited electron.

Measurements at low temperature and detailed calculations along the multiple scattering formalism are now in progress.

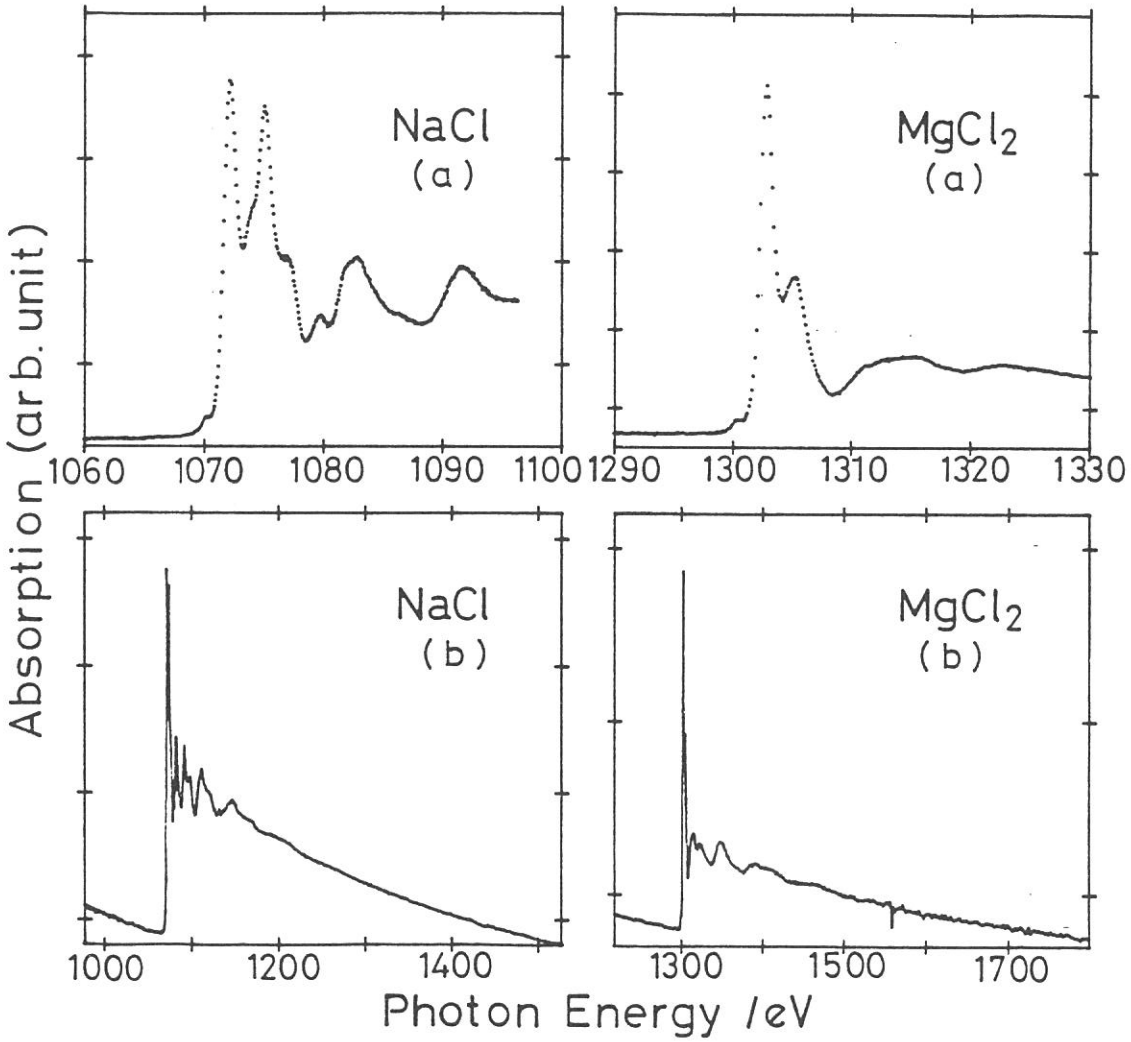

Fig. 1. K-edge spectrum of NaCl (a) XANES, (b) EXAFS.

Fig. 2. K-edge spectrum of $MgCl_2$ (a) XANES, (b) EXAFS.

Reference

1) T. Murata, T. Matsukawa, M. Mori, M. Obashi, S. Nao-e, H. Terauchi, Y. Nishihata, O. Matsudo, and J. Yamazaki, J. Physique Colloque C8 (1987) (in press).

XANES AND EXAFS STUDY ON DEHYDRATION PROCESS IN $Mg(OH)_2$

Yasuo NISHIHATA, Kazuya KAMON, Hirofumi SAKASHITA,
Hiromitu NAONO, Hikaru TERAUCHI, Takatoshi MURATA*,
Shun-ichi NAO-E**, Tokuo MATSUKAWA***, Masahiro MORI+,
Atsuo MATSUI++, and Ken-ichi MIZUNO++

Faculty of Science, Kwansei-Gakuin University, Nishinomiya 662
*Department of Physics, Kyoto University of Education, Kyoto 612
**College of General Education, Kanazawa University, Kanazawa 920
***College of General Education, Osaka University, Toyonaka 560
+College of General Education, Nagoya University, Nagoya 464
++Faculty of Science, Konan University, Kobe 658

Magnesium hydroxide $Mg(OH)_2$ is dehydrated to magnesium oxide MgO at high temperature. $Mg(OH)_2$ has a hexagonal layer lattice of CdI_2 type and MgO is of NaCl type. We feel so much interest in the $Mg(OH)_{2-2x}O_x$ system since the phase transition occurs by the dehydration. This system has been studied by x-ray diffraction technique[1] and it is found that the characteristic reflections of $Mg(OH)_2$ disappear at x_c=0.68 and the line broadings are observed near x_c. We are concerned with the local structure around the magnesium atoms and clarify the microscopic mechanisms of the dehydration in $Mg(OH)_2$.

The particles of $Mg(OH)_2$ (1000Å wide, 200Å thick) were dehydrated *in vacuo*. The degree of dehydration was determined from weight loss of $Mg(OH)_2$ by means of a vacuum electrobalance. Samples of $Mg(OH)_{2-2x}O_x$ with x=0.53, 0.71, 0.90, and 1.00 (MgO) were prepared by controlling temperature and heating time. The samples put in collodion which was dehydrated by molecular sieve. The top clean part of the solution was splashed on a nickel mesh.

X-ray absorption spectra near the Mg-K edge were taken by the use of the double crystal monochromator (DXM) constructed at BL-7A of UVSOR. Synchrotron energy was 750MeV. The intensity of the soft x-ray monochromatized by beryl crystals (2d= 15.97Å) was monitored with electron multiplier and the output current was lead into digital picoammeter.

Figure 1 shows the x-ray absorption spectra near the Mg-K edge of $Mg(OH)_{2-2x}O_x$ with x=0.00, 0.53, 0.71, 0.90, and 1.00. In the throuput transmission spectrum no structure appears near the Mg-K edge. On the other hand, there is a large anomalous dispersion near the Al-K edge since aluminium is one of the constituent elements in the monochromator crystals. Therefore, we can obtain the spectra up to about 250eV from the Mg-K edge when beryl crystals are used as monochromator. Apparently the spectra of $Mg(OH)_{2-2x}O_x$ with x=0.53, 0.71, 0.90, and 1.00 are almost the same. These spectra are distinct from that of $Mg(OH)_2$ concerning the spectrum just above the edge and the period of fluctuation. These results imply that the local structure around Mg atoms of the dehydrated samples is similar to that of MgO. The local structure of the sample with x=0.53 is also the MgO type though $Mg(OH)_{2-2x}O_x$ has a structure of $Mg(OH)_2$ below x_c=0.68 on an average. Detailed analysis is now in progress.

We are indebted to all the staffs of the UVSOR facility,

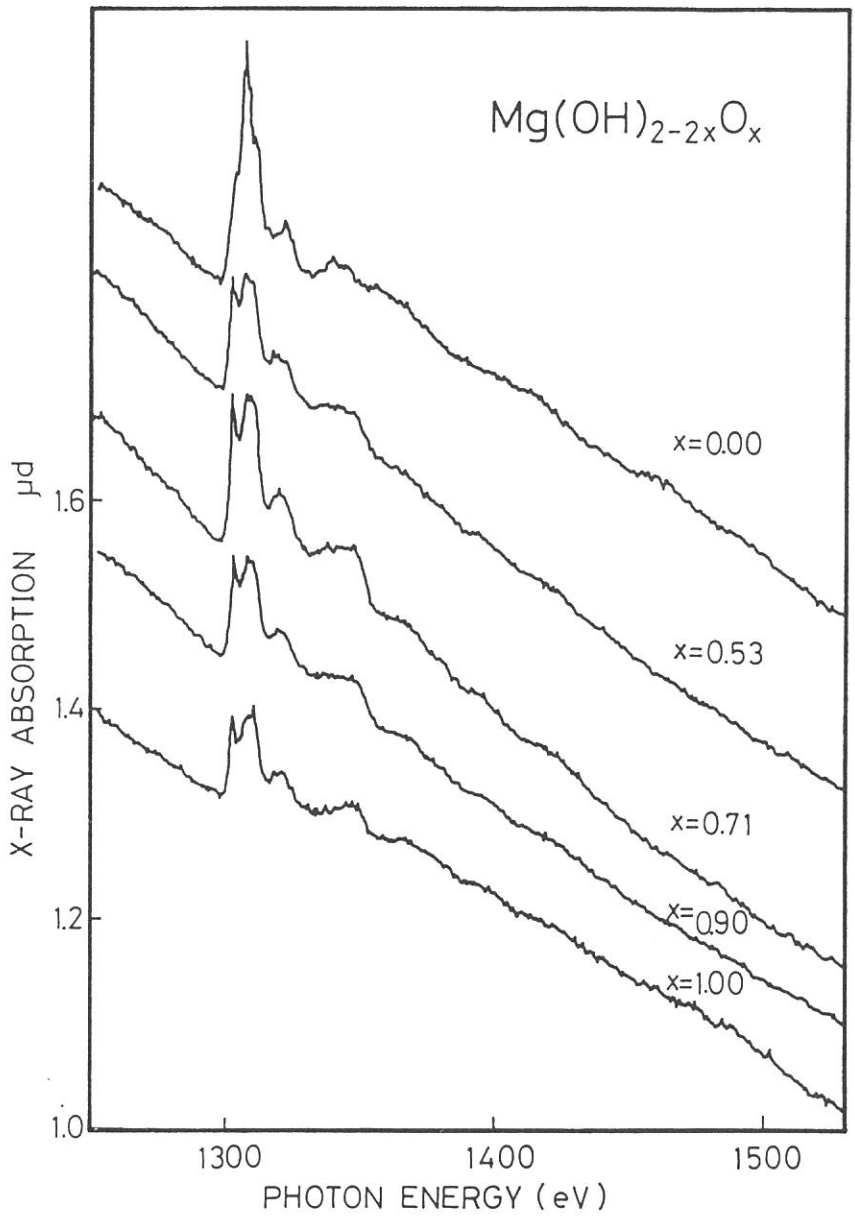

Fig. 1 X-ray absorption spectra near the Mg-K edge of $Mg(OH)_{2-2x}O_x$ with x=0.00, 0.53, 0.71, 0.90, and 1.00.

especially to Professor M. Watanabe, O. Matsudo, J. Yamazaki, and K. Fukui for their continuous support and encouragement through the work.

Reference

1) H. Terauchi, T. Ohga, and H. Naono, Solid State Commun. 35, 895 (1980).

INTRAMOLECULAR BAND MAPPING OF n-$CH_3(CH_2)_{34}CH_3$ AS A MODEL COMPOUND OF POLYETHYLENE

Hitoshi FUJIMOTO, Kazuhiko SEKI,* Nobuo UENO,**
Kazuyuki SUGITA,** and Hiroo INOKUCHI

Institute for Molecular Science, Myodaiji, Okazaki 444.
*Department of Materials Science, Faculty of Science,
Hiroshima University, Hiroshima 730.
**Department of Image Science and Technology,
Facuty of Engineering, Chiba University, Chiba 260.

The angle-resolved photoemission spectroscopy has an advantage in studying the electronic structures of oriented systems; the energy-band dispersion can be determined in addition to the density of states. We will report here on the preliminary angle-resolved UPS study of oriented films of hexatriacontane, n-$CH_3(CH_2)_{34}CH_3$, prepared by in situ vacuum evaporation using the synchrotron radiation of UVSOR as a tunable light source.

The oriented thin films of ~10 nm thickness were prepared in the preparation chamber (base pressre 10^{-9} Torr) and subsequently transferred to the main chamber. The detailed setup of the UPS system is reported in another article in this Report. Photoelectron spectra were measured for the normal emission from a sample surface with the incident angle of the light beam of 42°. The intramolecular energy-band dispersion was determined according to the method reported in Ref.1.

Figure 1 shows $h\nu$-dependent photoelectron spectra in the 30-65 eV photon energy region. Similar spectral changes at low photon energies ($\leq$54 eV) were already observed in the previous work,[1] but spectra at higher photon energies could not be measured. The experimental band structure obtained from these spectra is shown in Fig.2. As a guide for eyes, results of an ab initio calculation for a polyethylene chain by Karpfen,[2] which was 0.8 times contracted and shifted in an energy scale for a better fit, are also shown. The high-binding-energy bands of E_B=18 and 25 eV at k=0, which are assigned to C_{2s} bands, are smoothly connected at $k=\pi/a$, as expected theoretically.[2] This part could not be examined experimentally in the previous study.[1] It should be mentioned that these C_{2s}-originated bands become separated again at a higher photon energy of 74 eV (not shown in Fig.1).

In summary, we have presented a preliminary study of the angle-

resolved photoemission which covers the whole energy-band dispersion of oriented n-$CH_3(CH_2)_{34}CH_3$ films and demonstrated the powefulness of this technique for studying the intramolecular energy-band dispersion. Further detailed investigation is in progress on n-$CH_3(CH_2)_{34}CH_3$.

REFERENCES

1) K.Seki, N.Ueno, U.O.Karlsson, R.Engelhard, and E.-E.Koch, Chem. Phys., 105, 247(1986), and references therein.

2) A.Karpfen, J. Chem. Phys., 75, 238(1981).

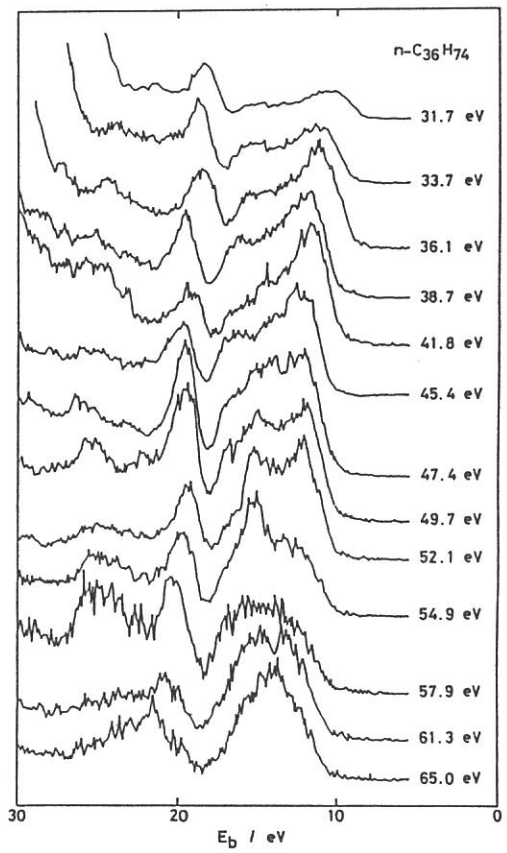

Fig.1 hν-dependent photoelectron spectra of n-$CH_3(CH_2)_{34}CH_3$.

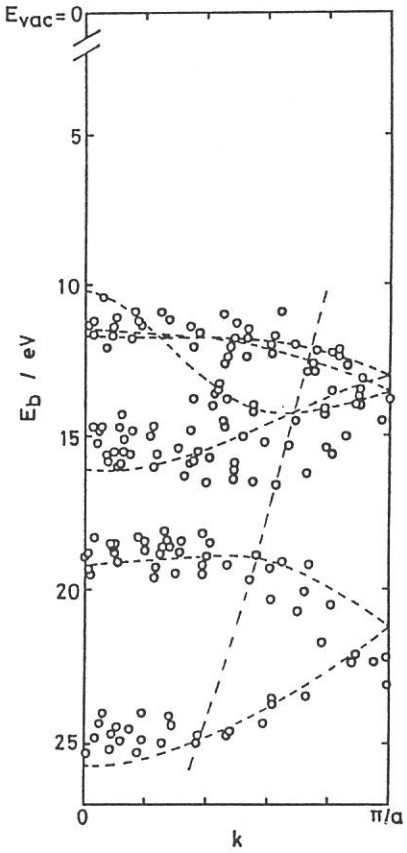

Fig.2 Energy-band dispersion of n-$CH_3(CH_2)_{34}CH_3$. The part at the right side of the broken line could not be accessed in the previous work.[1)]

PHOTON STIMULATED DESORPTION OF NEUTRAL SPECIES FROM LiF

Yoshitaka YAMADA, Tetsuji GOTOH*, Ayahiko ICHIMIYA, Yoichi KAWAGUCHI*, Masahiro KOTANI*, Shunsuke OHTANI*, Yahachi SAITO, Yukichi SHIGETA*, Shoji TAKAGI*, Yuji TAZAWA*, Goroh TOMINAGA* and Tsuneo YASUE

Department of Applied Physics, Nagoya University, Nagoya 464
*Institute of Plasma Physics, Nagoya University, Nagoya 464

In the previous work 1), we observed photon stimulated desorption (PSD) of positive ions from LiF. In the present work, we observed the desorption of neutral species from LiF and compared the energy dependence of PSD of neutral species with that of ions.

The experiments were carried out on BL6A2 of UVSOR. LiF (100) surface was cleaved in the air, and the specimen was mounted in a UHV chamber. The specimen temperature was held at 260 C during measurements in order to avoid electronic charging. The neutral species were ionized by electron impact with an energy of 30 eV and detected by a quadrupole mass spectrometer. The yields were normalized with the photon intensity.

Desorption yields of Li and HF were measured. The relative desorption yields of Li depended on the photon energy. The both yields of Li and HF gradually increased with the incident photon energy. Around the photon energy of 61 eV we reproducibly observed a sharp peak in the yield spectrum of Li as shown in fig. 1, while in the yield spectrum of HF no remarkable structures were observed in the same energy region.

For the desorption process of Li it is considered that the electronic processes are associated with the decay of the core-excitons. The sharp peak observed in the yield spectrum of neutral Li was located at the position of the strong peak in that of F^+ ions 1). Therefore the neutral Li desorption for the sharp peak is due to the interatomic Auger process such as

$$Li^{+*}+F^- \longrightarrow Li^*+F^++e^-, \qquad (1)$$

where asterisks indicate the core-excited states. Since the Li^* atoms interact weakly with the LiF crystal matrix, Li^* can easily desorb from the surface 2).

The broad background of the spectra showed quite different profiles from the yield spectra of the ions obtained previously 1). It is

considered that the desorption is due to migration of defects induced by photons as pointed out by Taglauer et al. 3) and Loubriel et al. 4).

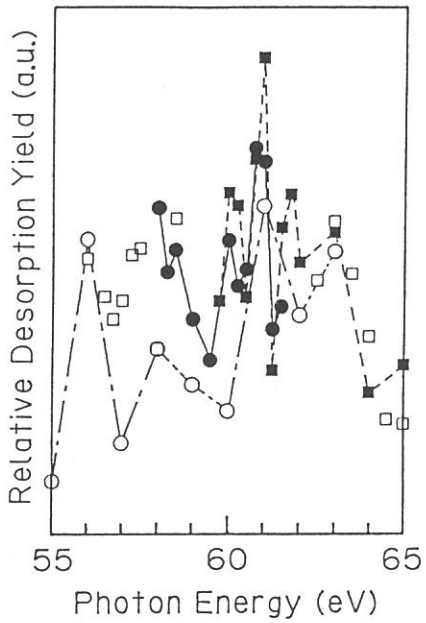

Fig.1. The relative Li yield spectra taken in several series of measurements around 61 eV, as shown with the different kind of plots and lines.

References

1) T. Yasue et al., Jpn. J. Appl. Phys. 25 (1986) L363.
2) N.H. Tolk et al., Phys. Rev. Lett. 49 (1982) 812.
3) E. Taglauer et al., Surf. Sci. 169 (1986) 267.
4) G.M. Loubriel et al., Phys. Rev. Lett. 57 (1986) 1781.

RADIATION-INDUCED DEGRADATION OF AMORPHOUS SILICON SOLAR CELLS

Akira YOSHIDA, Hiroyuki SUEZUGU, Tetsuya HIRANO,
Hiroshi OGAWA*, Hidehiko ITO*,and Takashi HIRAO**

Toyohashi University of Technology, Toyohashi, 440
*Saga University, Saga, 840, **Matsushita Electrical
Industrial Co.,Ltd., Osaka, 570

There is now considerable interest in the use of hydrogenated amorphous silicon(a-SiH) as one of the most promising materials for low cost solar cells, when prepared by decomposition of silane in a glow discharge. However, Staebler and Wronski (1) found that dark conductivity and photoconductivity are reduced significantly by prolonged illumination with intense visible light. These induced changes are found to be reversible and the original values are restored by annealing at temperature above 150°C. These metastable changes degrade the device characteristics. An understanding of the observed changes is crucial for the future applications. In this report, we show very rapid degradation of amorphous silicon solar cells exposed to synchrotron radiation beam.

Samples(p-i-n diodes) were prepared by glow discharge decomposition of SiH_4 gas on ITO-coated glass(Fig.1). Thicknesses of the p,i,and n layers were 10,400 and 40 nm, respectively. Another metal electrode of Al(70nm) or Ti(50nm) was deposited on the n layer, and used as a filter to synchrotron radiation beam. The short-circuit current of the sample exposed through the metal electrode was measured, showing very rapid decrease only in several seconds (Fig.2). Under illumination of the visible light in the SR beam (through a glass filter), no change in the I-V characteristics was observed (the curve at t=0 in Fig.3). But the degraded cell exposed to the beam with shorter wavelength has smaller output current and voltage, shown in Fig.3. Figs.4(a) and (b) represent a typical evolution after irradiation of the dark I-V characteristics. In Fig.4(a), the forward-bias current in the low bias range increases rapidly, and the diode quality factor becomes from 1.17 to 1.49. Large increase in the reverse-bias current was induced (Fig.4(b)). Fig.5 shows the I-V characteristics under illumination of white light of 5.4 mW/cm^2. Degraded characteristics recovered gradually even when kept in air at room temperature after exposure. Annealing at 75°C made them restored nearly to the original values. The degradation of p-i-n diodes is due to the increase in density of states caused by the beam.

(1) D.L.Staebler and C.R.Wronski, Appl. Phys. Lett. 31 292 (1977)

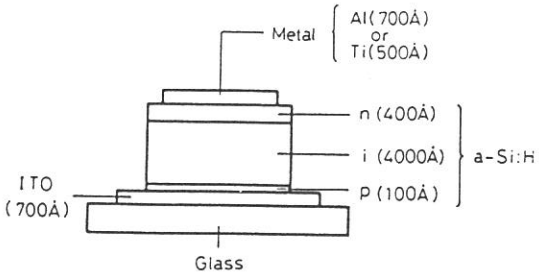

Fig.1 Sample(p-i-n diode)

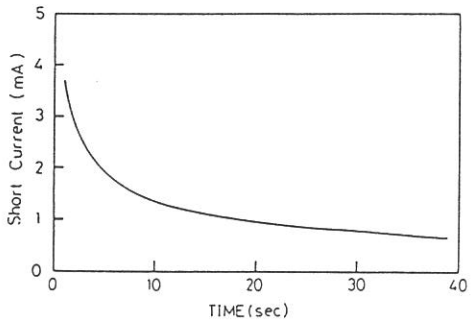

Fig.2 Time dependence of short-circuit current

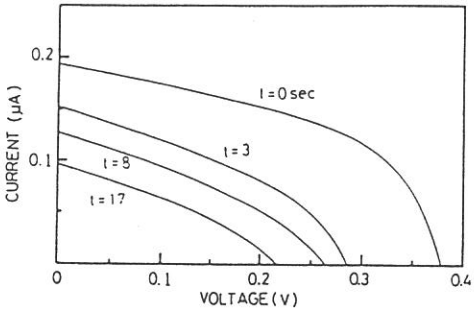

Fig.3 I-V characteristics under illumination of visible light in the SR beam

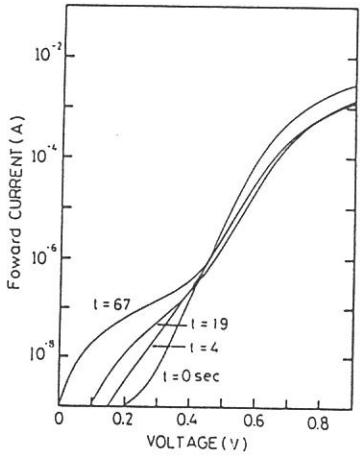

Fig.4(a) Dark forward-bias current

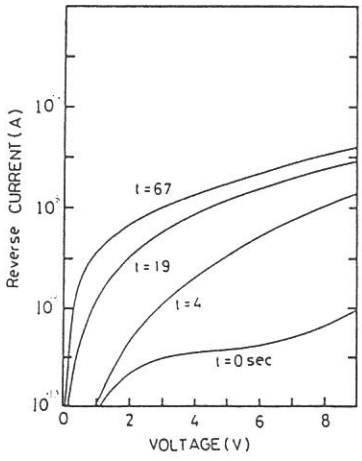

Fig.4(b) Dark reverse-bias current

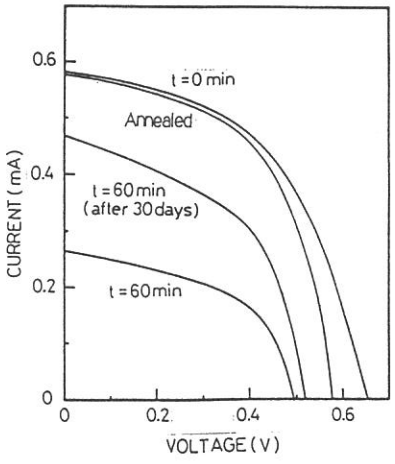

Fig. 5 Illuminated I-V characteristics ($5.4\ mW/cm^2$)

X-RAY VACUUM LITHOGRAPHY

Hitomi YAMADA, Takao SATO, Satoshi ITOH, Shinzo MORITA and Shuzo HATTORI
Department of Electronics, Nagoya University, Chikusaku Nagoya 464

X-ray lithography is one of the most promising technology to fabricate microelectronis circuit fabrication. Several efforts have been made to confirm the effectiveness of X-ray lithography. Synchrotron Radiation (SR) is supposed to be usefull, because the flux of usable X-ray from SR is large compared with other X-ray sources and SR is also highly collimated. Therefore, SR was used in this work.

The resists were decomposed randomly by SR exposure resulting in reduction of film thickness, which is known as self development. Dependence of self development characteristics of resists on SR wavelength was investigated in this experiment. SR exposure to resists was performed under the condition of 600 MeV and a current of 30 mA. For division of SR wavelength, polyimide and Be film were used as X-ray filters. The typical radiation is shown in Fig.1.

As the resists, plasma polymerized resists and conventional resists for comparision were used. Plasma polymerized resists were formed in an inductively coupled gas flow type reactor using methyl methacrylate (MMA) amd MMA with tetramethyl tin (TMT), SF_6, or styrene as monomers. The polymer structure of resists were investigated by IR and ESCA. ESCA results showd a smsll amount of Sn, S and F were incorporated into the polymer.

Self development characteristics are shown in Fig.2 for PMMA and in Fig.3 for PPMMA as a function of exposure dose. It was found that the removed thickness was increased linearly at low doses region, while it was saturated completely at high doses region for direct exposure. For exposure through X-ray filters, the removed thickness was linearly increased without saturation and exceeded the saturated region. Self development characteristics in a soft X-ray region are shown in Fig.4 for plasma polymerized resists. The self development was enhanced significantly by doping Sn, S and F as sentizers. The self development of PBS was more effectively developed than that of PMMA, which is considered to be attributed to be high G value of PBS.

In ordre to investigate the mechanism of self developmen, IR and ESCA measurement were performed before and after exposure. Also, the decomposed products released from film were detected by mass spectroscopy.

From these results, it was found that the change of molecular structure was varied by SR wavelength region. Therefore, the self development characteristics were changed under both exposure conditins. Recombination reaction was actively induced by direct exposure and the molecular structure which was hard enough to withstand to SR exposure was formed. By using X-ray filters, decomposition connecting with self development was more effectively advanced than that for direct exposure.

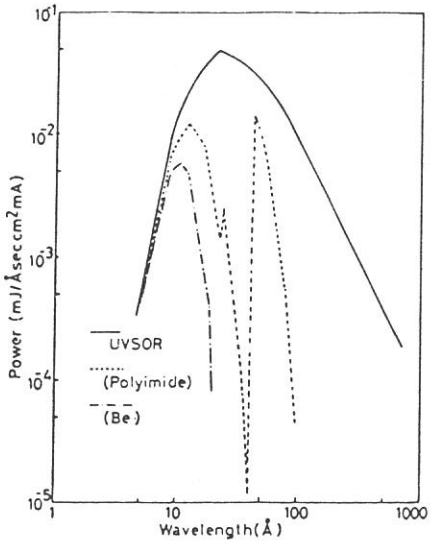

Fig.1 Sr wavelength distribution

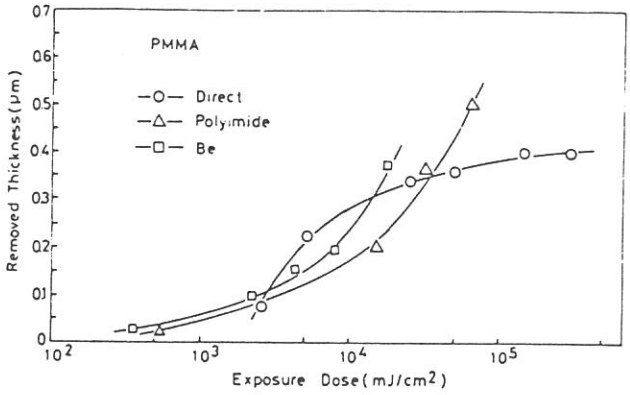

Fig.2 Self development characteristics of PMMA

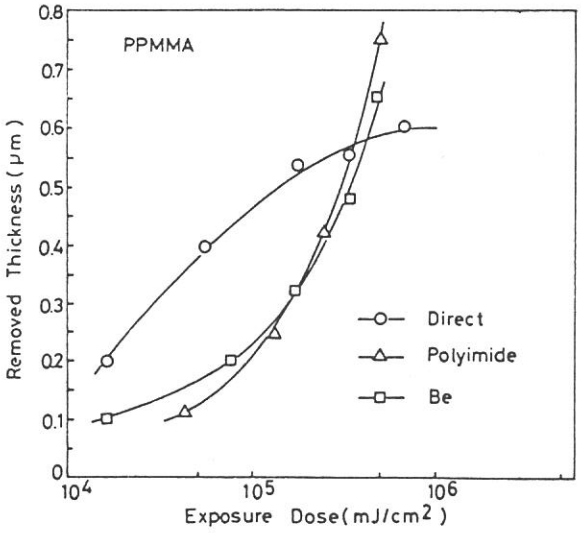

Fig.3 Self development characteristics of PPMMA

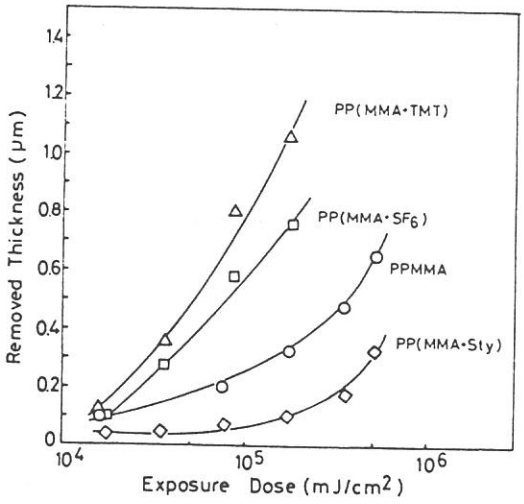

Fig.4 self development characteristics of plasma polymerized resists in a soft X-ray region

CHARACTERISTICS OF MULTILAYER REFLECTORS IN 80-300A REGION

Koujun YAMASHITA, Hiroshi TSUNEMI, Akira MIYAKE,
Yoshiaki KATO*, Hiroyuki SHIRAGA*, Takuma ENDO*,
and Katsuya KAMEI*

Department of Physics, Osaka University, Toyonaka 560
*Institute of Laser Engineering, Osaka University, Suita 565

The development of multilayer reflectors makes it possible to fabricate the normal incidence x-ray telescope and the x-ray laser mirror in the wavelength region 40-300A. The multilayer reflector is the most promising optical element to get the high reflectivity for the normal incidence, although the sensitive wavelength band is limited to $\lambda/10$. It is also possible to apply it for the x-ray spectrometer and polarizer.

The measurement of reflectivities of multilayer reflectors was carried out with the monochromatized synchrotron radiation in 80-300A region on BL-6A2. The incident beam is monochromatized with the plane grating monochrometer and introduced to the reflectometer. The multilayer is mounted on the rotation axis and the detector(sodium salicylate sprayed photomultiplier) on the rotation arm. The incidence angle is changed from 10° to 85° by 5° step, which is measured from the the normal of the reflecting surface. The rotation axis of the reflectometer is perpendicular to that of the grating, so that we can mostly measure the reflectivity of p-polarized beam. However the reflectivity for the normal and grazing incidence does not much depend on the degree of polarization. Multilayer reflectors, such as Mo/Si, W/C, Ni/C and Ru/Si with 2d=112-250A and 5-60 layer pairs, were evaluated with this system by measuring the peak reflectivity, the wavelength resolution and Bragg angle. The peak reflectivity of Mo/Si(2d=226A, N=60) was obtained to be 37% at 212.6A for the first order and 5% at 113.7A for the second order at the incidence angle 10°, as shown in Fig.1. That for the incidence angle is shown in Fig.2, which shows minimum reflectivity at 45° and sharp decrease at Si-L edge (123A). Open circles are values corrected for the contribution of the second order caused by the grating. In the wavelength range 80-150A, the incident beam is purely first order, whereas that in the longer wavelength range than 150A is contaminated with the second order beam. This contribution is evaluated with

the wavelength scan at the fixed incidence angle. If the second order is dominant, we can observe the second peak at the wavelength just as twice as the fist order, which is longer than 2d value.

The observed peak reflectivities are compared with values calculated with optical constants. Barbee et al.[1] reported that the peak reflectivity of Mo/Si was 50% at 170A in the near normal incidence and was higher than the theoretical value. We have to investigate the quality of multilayer reflectors, taking into account the opical constant, the surface roughness of substrate and the interfacial roughness of each layer.

Reference

1) T.W. Barbee,Jr, S. Mrowka, and M.C. Hettrick, Appl. Opt. 24 (1985) 883.

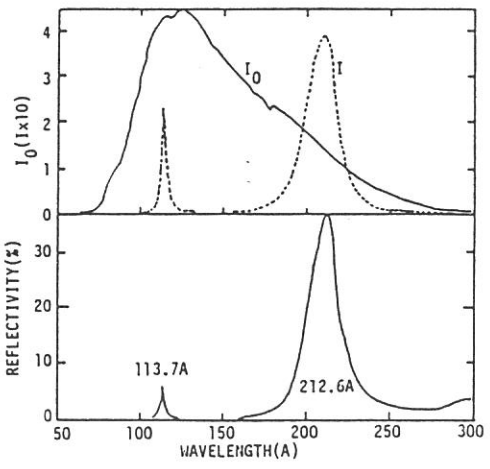

Fig.1 Reflectivities of Mo/Si (2d=226A, N=60) at the incidence angle 10°. I_0: incident beam I: reflected beam.

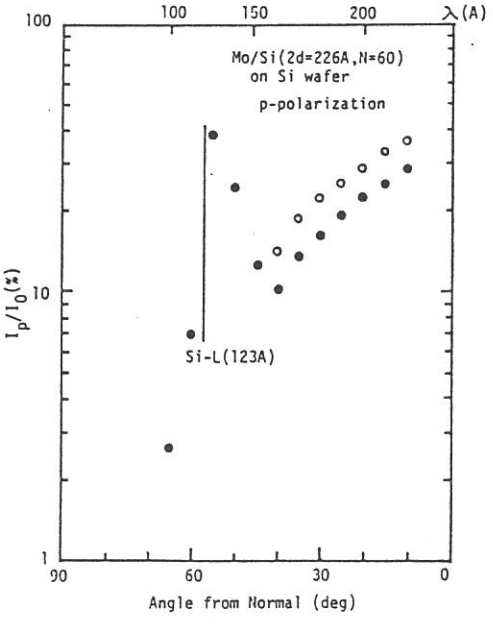

Fig.2 Peak reflectivities vs. the incidence angle. Open circle: corrected for the second order.

Focusing Test of Free Standing Zone Plate in VUV Wavelength Region

Yutaka Watanabe[1),4)], Shigetaro Ogura[1)], Yoshinori Nagai[2),4)], Yasushi Nakajima[3)], and Hiroshi Kihara[4)]

1)Electronic Material Division, Research Department 34, Canon INC., Atsugi 243-01, 2)Laboratory of Molecular Biology, School of Veterinary Medicine, Azabu University, Sagamihara 229, 3)Department of Physics, Waseda University, Shinjuku-ku, Tokyo 160, 4)Department of Physics, Jichi Medical School, Minamikawachi - machi, Tochigi 329-04

A free standing zone plate was fabricated as an optical element of X-ray microscope, and was tested at UVSOR beam line BL6A2 at Institute for Molecular Science. The zone plate was designed for observing biomolecules in VUV wavelength region [1] with features of 150 mm in focal length at 80 Å, about 1000 μm in diameter, 1.2 μm in outermost zone width, and 104 in the number of transparent zones. Optical arrangement of the test system is shown in Fig.1, where an electron multiplier (for one-dimensional intensity distribution) or photographic films (for two-dimensional intensity distribution) is used.

After X-ray passed through the pinhole and the zone plate, the intensity at the slit plane was measured by the electron multiplier (Hamamatsu PhotonicsR595) and by sliding the slit across the X-ray beam. In Fig.2 the intensity distribution of X-ray at 145.7 Å is shown with a hole of 1mm ϕ instead of the zone plate in Fig.1. Figure 3 shows the intensity distribution of X-ray at 145.7 Å with the zone plate, whereas Figure 4 shows the intensity distribution at 145.7 Å, sliding the zone plate by 0.4 mm toward y-axis. The central part of Fig.3 is contributed by mainly the zeroth order diffraction from the zone plate, and by sharp peaks probably due to the other order diffractions by the zone plate.

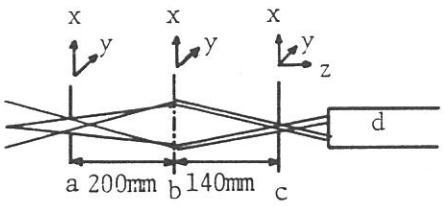

Fig.1 Test system a:pinhole b:zone plate c:slit or photographic film (in film's case $\overline{ab}$=264.4mm, $\overline{bc}$=235.9mm) d:electron multiplier

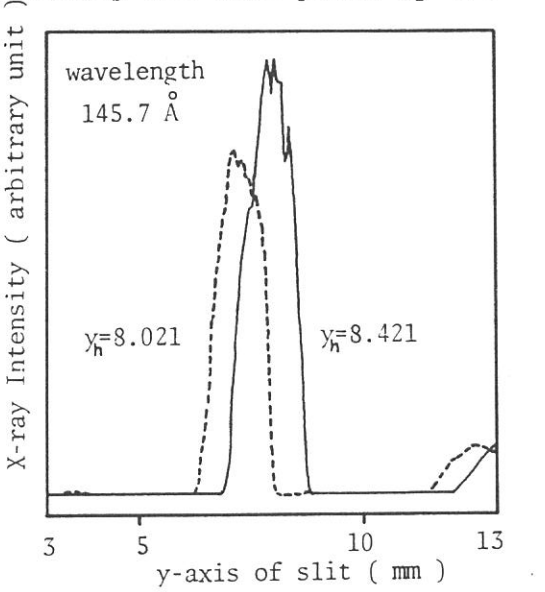

Fig.2 Intensity distribution with a hole of 1 mm ϕ
y_h: y-axis of a hole

At the same time, the two-dimensional distribution of 96.2 Å X-ray through the zone plate was taken with a photographic film (minicopy ASA 32),shown in Fig.5. X-ray intensity of the film was measured densitometrically (Fig.6). High intensity at the center of the film may indicate the focusing of the first order diffraction.

[1] Y.Nagai,Y.Nakajima,Y.Watanabe,S.Ogura,K.Uyeda,Y.Shimanuki,and H.Kihara,Proceedings of X-ray Microscopy '86,Springer-Verlag, (1986) in press.

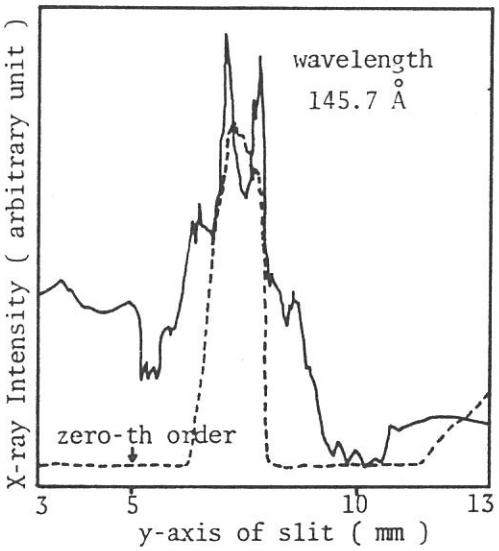

Fig.3 Intensity distribution with the zone plate (zone plate y=8.021 mm)

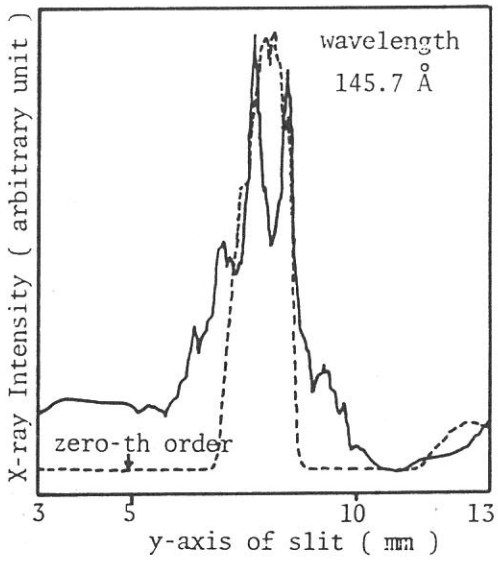

Fig.4 Intensity distribution with the zone plate (zone plate y=8.421 mm)

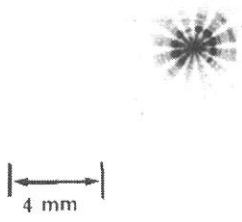

Fig.5 Two-dimensional distribution

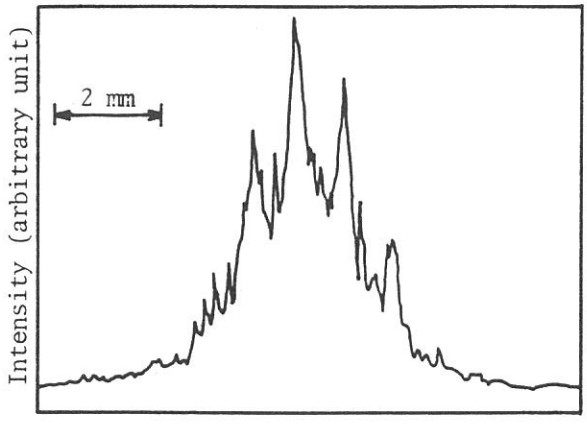

Fig.6 densitometrically scanned intensity distribution

Measurement of a far infrared pulse width by Fourier transform spectroscopy

Tetsuhiko OHBA and Shun-ichi IKAWA

Department of Chemistry, Faculty of Science,
Hokkaido University, Sapporo 060, Japan

The pulse width of the far-infrared radiation from UVSOR has been estimated to be about 0.5 nsec at least from a measurement of interference fringes due to a hyperpure silicon plate of 0.3 cm thickness by use of a Martin-Puplett interferometer installed at BL6A.

Because of a spatially finite length of the pulsed radiation, the interference efficiency will decrease with increasing optical path difference between two arms of the interferometer. The shape of the radiation pulse from UVSOR can be approximated by a Gaussian funtion, so that the relative interference efficiency at a path difference, x, is given by $\exp[-(\ln 2/a^2)x^2]$, where a is the length of the pulse. Consequently, the observed interferogram can be expressed as,

$$I_p(x) = I(x)\ \exp[-(\ln 2/a^2)x^2], \qquad (1)$$

where I(x) is the interferogram to be observed at $a=\infty$. Therefore, the effect of the finite pulse width on the interferogram is similar to the apodization and the related instrument line shape function is given by,

$$B_i(\nu) = \int_{-L}^{L} \exp[-(\ln 2/a^2)x^2]\ \mathrm{COS}2\pi\nu x\ dx, \qquad (2)$$

where L is the maximum optical path difference. The shapes of $B_i(\nu)$ for several pulse widths are shown in Fig.1. It is easily seen that the spectral resolution lowers as the pulse width becomes comparable to or less than the maximum path difference.

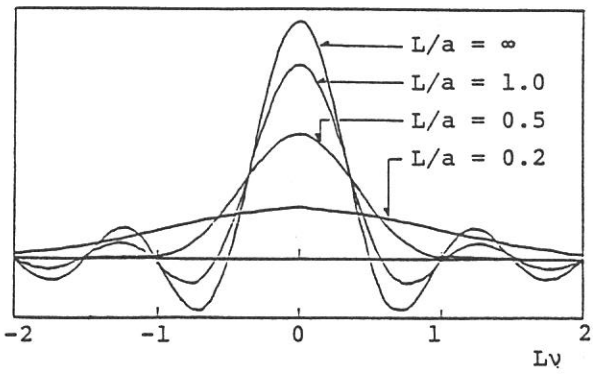

Fig.1 Instrument line shape functions for gaussian pulsed source.

The observed spectrum is given by the Fourier transform of Eq.(1) and

can be written as,

$$B_p(\nu) = \int_{-\infty}^{\infty} B(\nu') \, B_i(\nu-\nu') \, d\nu', \qquad (3)$$

where $B(\nu') = \int_{-\infty}^{\infty} I(x) \, \cos 2\pi\nu' x \, dx$

is the true spectrum.

Fig.2 shows the observed interference fringes due to the silicon 0.3 cm window in the 25-40 cm^{-1} range measured at L=5.12 cm. The average amplitude of the observed fringes is estimated to be 64.6%. A theoretical calculation of the spectrum, $B_p(\nu)$, was carried out for several pulse widths using the optical constants of hyperpure silicon, and are listed in Table 1. Uncertainty or spread of the incident angle of the radiation on the window and imperfectness in the flatness and the parallelism of the window surfaces were not taken into the calculations. Though these effects should be small in the present measurement, they will always reduce the amplitude of the fringes to a certain extent. Thus we conclude from Table 1 that the pulse width of the far-infrared radiation is about 0.5 nsec at least.

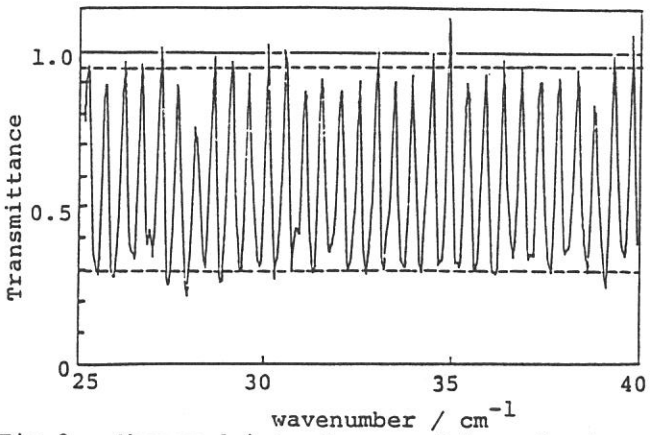

Fig.2 Observed interference fringe due to silicon 0.3cm window measured at L=5.12cm. The broken lines indicate the average amplitude.

Table 1 Calculated amplitudes of the interference fringes due to silicon 0.3cm window for several pulse widths.

Width/cm	Duration/nsec	Amplitude/%
∞	∞	65.3
25.6	0.85	64.9
20.48	0.68	64.7
15.36	0.51	64.3
10.24	0.34	63.0
5.12	0.17	57.7
2.56	0.08	41.5
observed		64.6

Measurement of the far infrared optical constants of liquid acetonitrile

Tetsuhiko OHBA and Shun-ichi IKAWA

Department of Chemistry, Faculty of Science,
Hokkaido University, Sapporo 060, Japan

The far-infrared optical constants of liquid acetonitrile were determined from a transmission spectrum measured by use of a far-infrared interferometer at BL6A.

For normal incidence, a transmittance of a liquid cell as shown in Fig.1, is given by,

n_1	Air	
$\hat{n}_2$	Window	d_2
$\hat{n}_3$	Sample	d_3
$\hat{n}_4=\hat{n}_2$	Window	d_4
$n_5=n_1$	Air	

Fig.1 A liquid cell.

$$T_5(\nu) = \left| \frac{(1-\hat{r}_{12}^2)(1-\hat{r}_{23}^2)e^{i(\hat{\beta}_2+\hat{\beta}_3+\hat{\beta}_4)}}{1+\hat{Q}} \right|^2 , \qquad (1)$$

where $1 + \hat{Q} = 1 + \hat{r}_{12}\hat{r}_{23}(e^{2i\hat{\beta}_2}+e^{2i\hat{\beta}_4}-e^{2i\hat{\beta}_2+2i\hat{\beta}_3}-e^{2i\hat{\beta}_3+2i\hat{\beta}_4})$

$$- \hat{r}_{23}^2 e^{2i\hat{\beta}_3} - \hat{r}_{12}^2 e^{2i\hat{\beta}_2+2i\hat{\beta}_3+2i\hat{\beta}_4} + \hat{r}_{12}^2\hat{r}_{23}^2 e^{2i\hat{\beta}_2+2i\hat{\beta}_4} ,$$

$$\hat{r}_{ij} = \frac{\hat{n}_i - \hat{n}_j}{\hat{n}_i + \hat{n}_j} , \qquad \hat{\beta}_i = 2\pi\hat{n}_i\nu d_i , \qquad \hat{n}_i = n_i + ik_i .$$

The observed transmittance is given by the convolution of Eq.(1) with the instrument line shape function, $f(\nu)$, as,

$$T_{obs}(\nu) = \int_0^\infty T_5(\nu') f(\nu-\nu') d\nu' . \qquad (2)$$

In Eq.(2), unknown parameters are the complex refractive indices of the sample, $\hat{n}_3(\nu) = n_3(\nu) + ik_3(\nu)$, because all the other variables could be measured separately. In addition, $n_3(\nu)$ is related with $k_3(\nu)$ by the Kramers-Kronig relation,

$$n(\nu) = n(\nu_r) + \frac{1}{2\pi^2} P\int_0^\infty \frac{\alpha(x)}{x^2-\nu^2} dx - \frac{1}{2\pi^2} P\int_0^\infty \frac{\alpha(x)}{x^2-\nu_r^2} dx , \qquad (3)$$

where $\alpha = 4\pi\nu k$ and $n(\nu_r)$ is the refractive index at the anchor point. We assumed for the absorption coefficient the following analytical form,

$$\alpha(\nu) = \frac{\nu^2}{P_0 + P_1\nu^2 + P_2\nu^4 + P_3\nu^6 + \cdots\cdots + P_N\nu^{2N}} \qquad (4)$$

This expression is identical with the spectral density of the continued-fraction representation by Mori, which gives quantum statistically exact result at the limit of $N=\infty$.

Using Eqs.(1)-(4), we performed the simulation of the observed transmittance. N was taken to be 6, and the adjustable parameters were P_0-P_6, d_3, and the difference in thickness between two silicon windows, Δd_{24}. The best fit obtained for neat CH_3CN is shown by a solid curved line in Fig.2. The agreement between the observed and calculated values is excellent. Two types of interference fringes are seen in Fig.2; one ($\Delta\nu$=30cm^{-1}) is explained by Δd_{24} (=0.05mm) and the other ($\Delta\nu$=130cm^{-1}) by d_3 (=0.03mm). This is the first observation of the former kind of fringes as far as we know. This fact and the successful simulation without any other effect, such as a spread of a incident angle of the radiation, are owing to a good coherency of the radiation from UVSOR. In Fig.3, the absorption coefficient of neat CH_3CN determined in the present work is compared with several literature data recently reported. The present result agrees very well with the laser ATR result from Ref.1.

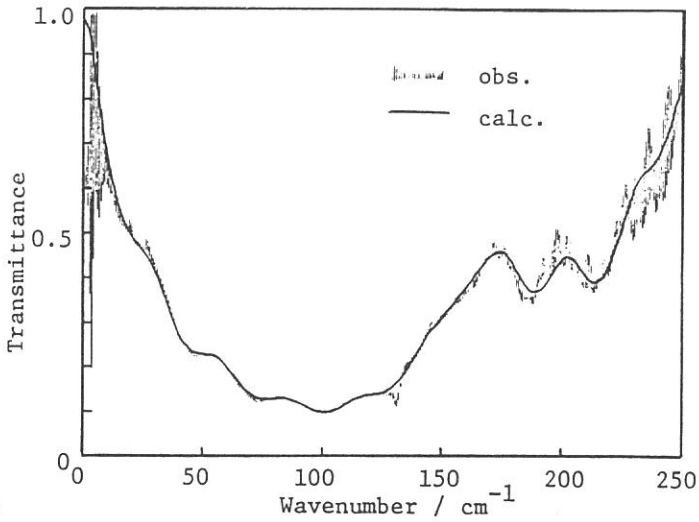

Fig.2 Transmittance of acetonitrile.

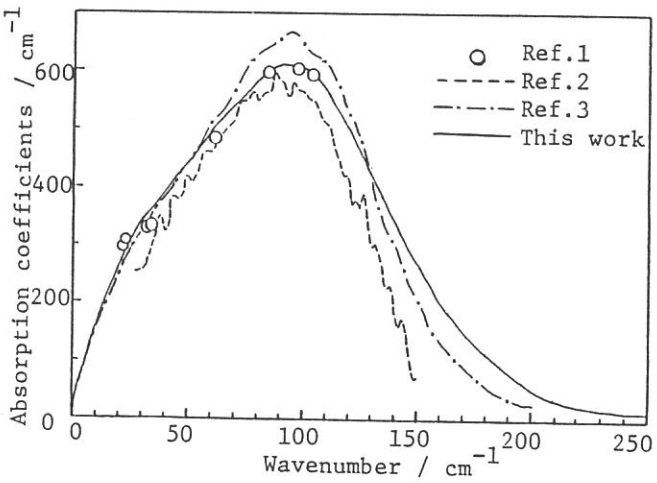

Fig.3 Absorption coefficients of acetonitrile.

References

1. S.Ikawa et al. Intern.J.Infrared Millimeter Waves, 6, 287(1985)
2. J.R.Birch et al. Chem.Phys.Lett., 117, 197(1985)
3. K.E.Arnold et al. Molec.Phys., 48, 451(1983)

FAR-INFRARED SPECTROSCOPY OF SMALL SOLID STATE SPECIMENS

Takao NANBA, Yasuhito URASHIMA, Mikihiko IKEZAWA,
Makoto WATANABE* and Hiroo INOKUCHI*

Department of Physics, Tohoku University, Sendai 980
*Institute for Molecular Science, Myodaiji, Okazaki 444

One of the most useful characteristics of the system of far-infared spectroscopy by synchrotron radiation at the beam line BL6A1 is that the size of the light beam for measurement is very small. The cross sectional diameter of the light beam is as small as 3 mm at the position of the specimen.[1] Therefore, one can observe the reflectivity or transmission spectrum using a small specimen. Moreover, the light is linearly polarized and the spectroscopic system is convenient for the observation of anisotropic materials.

(I) Alkali silver halide crystals

The alkali silver halide crystal has the orthorhombic structure.[2] Reflectivity spectra of Rb_2AgI_3 and K_2AgI_3 crystals were measured with the normal incidence configuration at 300, 80 and 15 K. Examples of spectra of Rb_2AgI_3 are shown in Fig.1. The diameter of the measuring light beam was 2 mm. The light was polarized along the three directions of the crystal. A number of lines were resolved and the reflectivity spectra were analyzed to obtain the dielectric constants by the Kramers-Kronig analysis.

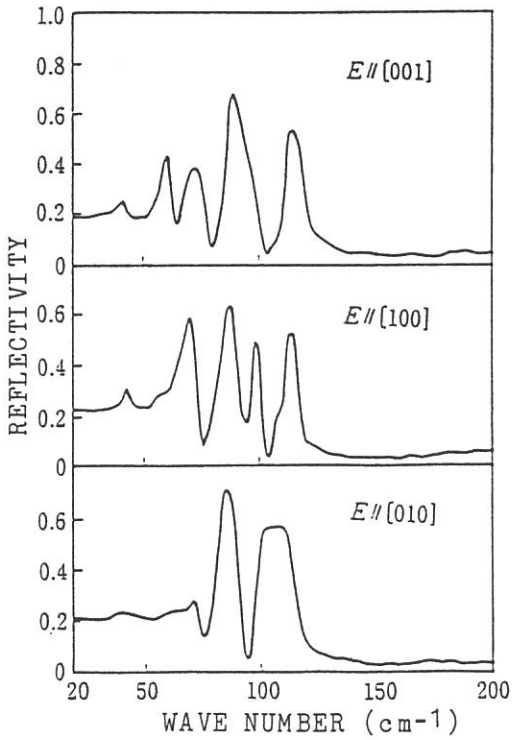

Fig.1 Reflectivity spectra of Rb_2AgI_3 crystal at 80 K. The diameter of measuring light beam is 2 mm and the electric vector is parallel to the crystal axes.

(II) Black phosphorus crystal

The black phosphorus crystal has two infrared active modes of the lattice vibration.[3] We have observed the B_{1u} mode in the far-infrared region with a high resolution of $\Delta\nu=0.3$ cm^{-1}. In Fig.2 reflectivity spectra at 300 and 15 K are shown. The light for measurement was polarized along the x-axis[3] of the crystal.

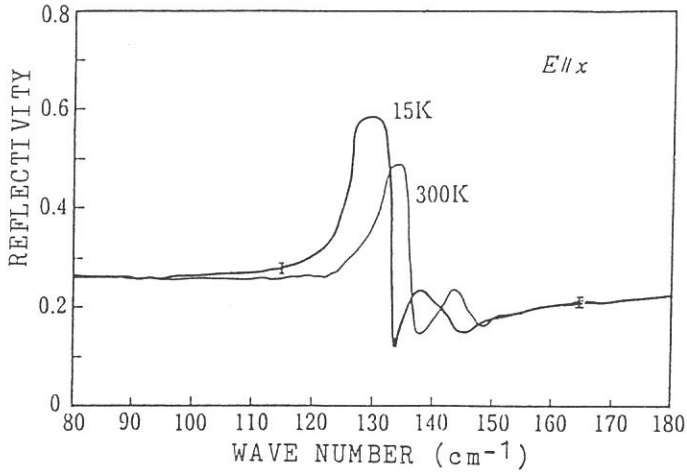

Fig.2 Reflectivity spectra of black phosphorus crystal. The diameter of the measuring light beam was 4 mm and the spectral resolution $\Delta\nu=0.3$ cm^{-1}.

By Kramers-Kronig analysis of the spectra dielectric constants were obtained. From a peak of the spectrum of ε_2 the TO phonon energy was determined as 134.0 and 128.3 cm^{-1} at 300 and 15 K, respectively. The TO mode was found to shift to the low energy side at low temperature. The temperature dependence explains a discrepancy between reported values[4,5] of the TO phonon energy. From the peak of the loss function, the energy of the LO mode at 15 K was determined as 133.6 cm^{-1}. Then the TO-LO splitting energy is 5.3 cm^{-1}. This value is about three times larger than a previously reported value[5] but is in good agreement with the theoretically calculated value[6] of 6 cm^{-1}.

References

1) T.Nanba, Y.Urashima, M.Ikezawa, M.Watanabe, E.Nakamura, K. Fukui and H.Inokuchi: Int. J. Infrared and Millimeter Waves 7(1986)1769.
2) K.Edamatsu, M.Ikezawa, H.Tokailin, T.Takahashi and T.Sagawa: J. Phys. Soc. Jpn. 55(1986)2880.
3) C.Kaneta, H.K.Yoshida and A.Morita: Solid State Comm. 44 (1982)613, J.Phys. Soc. Jpn. 55(1986)1213.
4) M. Ikezawa, Y.Kondo and I.Shirotani: J. Phys. Soc. Jpn. 52 (1983) 1518.
5) S.Sugai and I.Shirotani: Solid State Comm. 53(1985)753.
6) C.Kaneta and A.Morita: J. Phys. Soc. Jpn. 55(1985)1224.


UV
50R
T.O
E.N
H.Y
K.F
J.Y
O.H
M.H
K.S
T.K
T.K
H.L
M.W